SUPPORTING INFORMATION

N acyl-benzenesulfonamide dihydro-1,3,4-oxadiazole hybrids: seeking for selectivity towards carbonic anhydrase isoforms

Giulia Bianco, Rita Meleddu, Simona Distinto, Filippo Cottiglia, Marco Gaspari, Claudia Melis, Angela Corona, Rossella Angius, Andrea Angeli, Domenico Taverna, Stefano Alcaro, Janis Leitans, Andris Kazaks, Kaspars Tars, Claudiu T. Supuran and Elias Maccioni.

Table of Contents

Chemistry

General methods

Reagents and solvents were obtained from commercial suppliers and were used without further purification. All melting points were determined by the capillary method on a Stuart SMP30 Digital Advanced apparatus and are uncorrected.

Structures, melting points, yields of the reactions and crystallization solvents of EMAC derivatives are reported in Table S1. Mass spectra were registered on a Q-Exactive mass spectrometer (Thermo Fisher Scientific, Germany). The Q-Exactive hybrid mass spectrometer was equipped with a nano-electrospray source operating

in negative ion mode (-700 V). For all the experiments, the ion transfer tube temperature was set at 250 °C while the S-Lens at 50.0. A full MS scan was acquired (0.3 min) in the Orbitrap analyzer at resolution of 140,000, within the *m/z* range of 100–800, and by using a target AGC value of 1.00×10^6. The maximum injection time was set at 500 ms. Compounds were dissolved in methanol to prepare stock solutions. Samples for flow injection were prepared by diluting stock solutions with a solution of water/acetonitrile 1/1 down to a concentration of 7-30 ppm. Sample solutions (5 μL) were loaded into borosilicate emitters for nano-electrospray (Thermo Fisher Scientific) and infused into the Q-Exactive MS. Found mass values are in agreement with theoretical ones (Table S2). Mass spectra are reported in Figures S1-13.
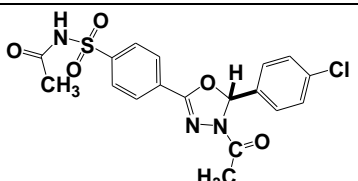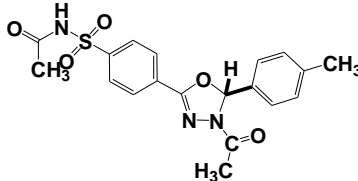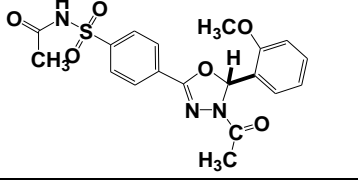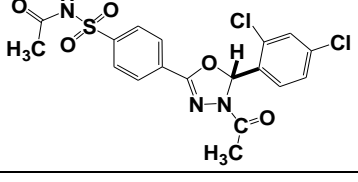
^{1}H-NMR and ^{13}C-NMR chemical shifts of compounds **EMAC8000a-m** are tabled in Table S3. NMR spectra are depicted in Figures S14-26.

All samples were measured in CDCl$_3$ or DMSO-d6 at 278.1 K temperature on a Bruker AVANCE III 400 MHz spectrometer. Chemical shifts are reported in ppm. Coupling constants *J* are expressed in hertz (Hz).

TLC chromatography was performed using silica gel plates (Merck F 254), spots were visualised by UV light. HPLC enantioseparation was conducted by means of a Varian 920 LH instrument fitted with an autosampler module with a 1000 μL loop. The analyses were monitored using a dual-wavelength UV detector settled at 254 and 366 nm. The enantioseparation was performed using Chiralpak IA (250 x 4.6 mm I.D. and 250 X 10 mm I.D.) columns (Chiral Technologies Europe, Illkirch, France). HPLC-grade solvents were supplied by VWR International.

Specific rotations of stereoisomers of (-)-**EMAC8000d** and **(+)-EMAC8000d** dissolved in acetonitrile, were measured at 589 nm (25° C) by a Perkin Elmer 241 polarimeter equipped with a Na lamp.

Table S1. Chemical, analytical, and physical data of derivatives **EMAC 8000a-m**.

Compound	Structure	M.P. °C	Yield %	Aspect	Cryst. solvent
EMAC8000a		220	63	white	ethanol
EMAC8000b		184-186	55	white	ethanol
EMAC8000c		213	54	creamy	ethanol
EMAC8000d		222-224	71	creamy	ethyl acetate

Compound	Structure	mp (°C)	Yield (%)	Color	Solvent
EMAC8000e		200-202	63	white	ethanol
EMAC8000f		231-233	74	creamy	ethyl acetate
EMAC8000g		199-202	60	creamy	ethanol
EMAC8000h		197-199	94	creamy	ethyl acetate
EMAC8000i		244-246	58	white	ethanol
EMAC8000j		199-202	63	creamy	ethanol
EMAC8000k		172-174	69	white	ethanol
EMAC8000l		173-176	90	white	isopropanol
EMAC8000m		257-259	93	white	ethanol

Mass spectra of compounds EMAC8000a-m
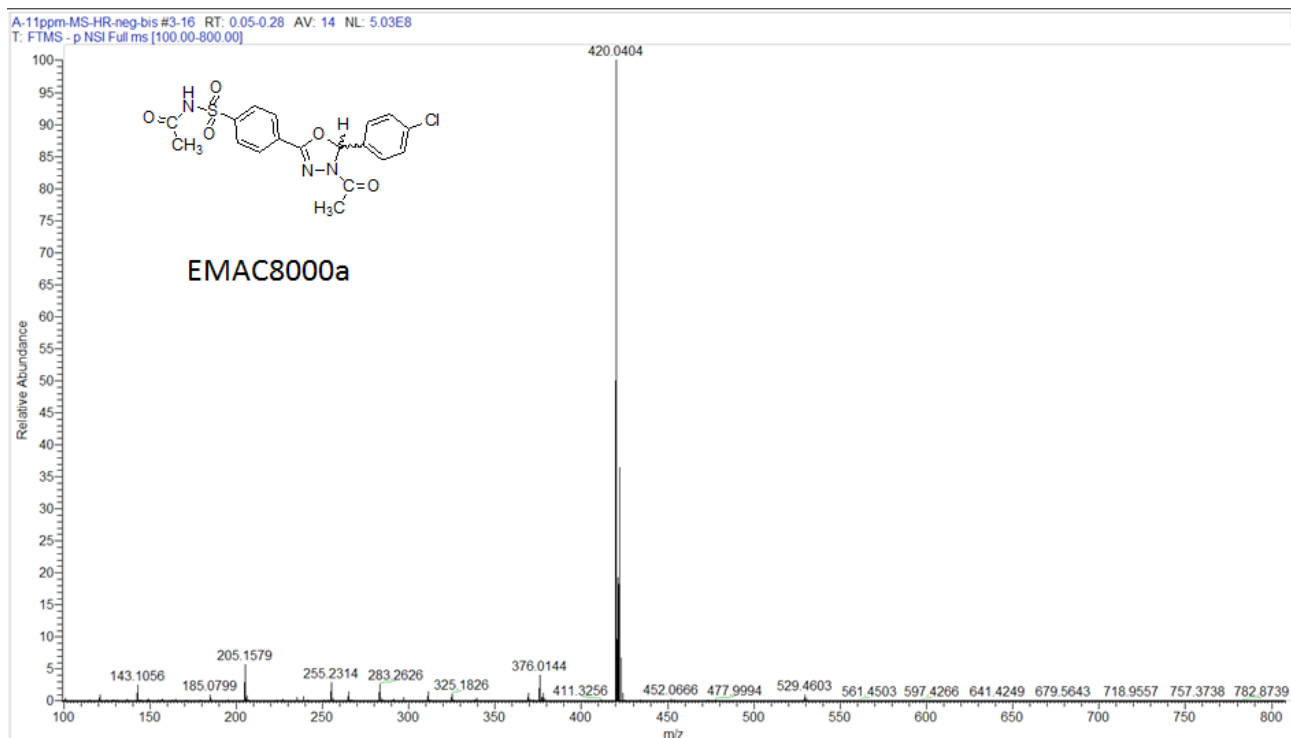
Figure S1. Full Mass Spectrum of compound **EMAC8000a**. Theoretical *m/z*: 420.0426, [M-H]⁻; accuracy: -5.2 ppm.
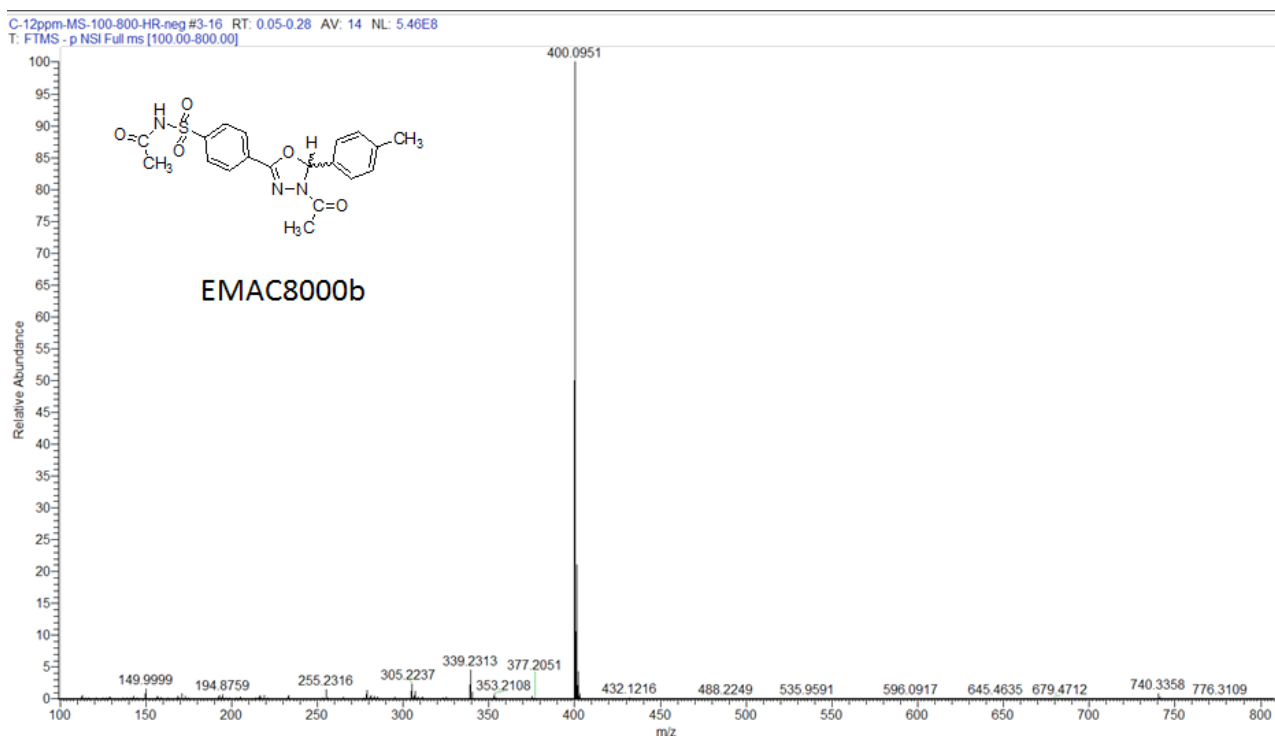
Figure S2. Full Mass Spectrum of compound **EMAC8000b**. Theoretical *m/z*: 400.0973, [M-H]⁻; accuracy: -5.5 ppm.

4
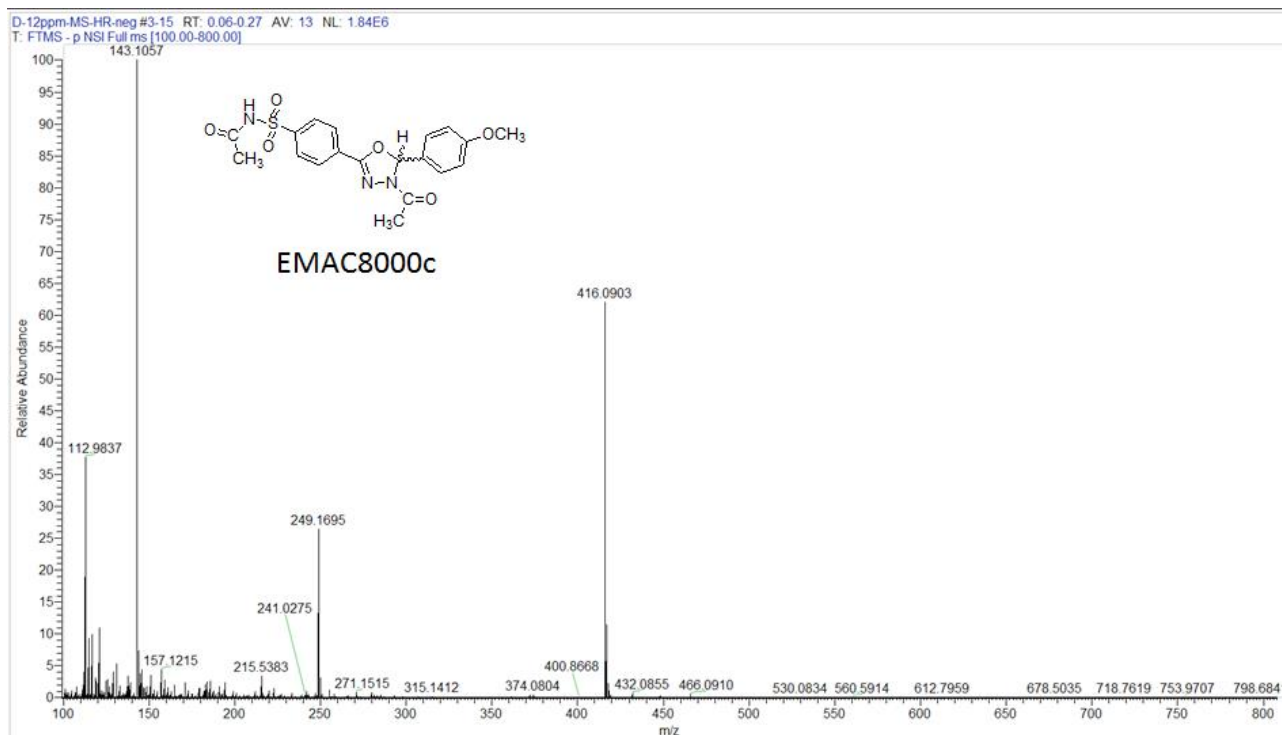
Figure S3. Full Mass Spectrum of compound **EMAC8000c**. Theoretical *m/z*: 416.0922, [M-H]⁻; accuracy: -4.6 ppm.

Figure S4. Full Mass Spectrum of compound **EMAC8000d**. Theoretical *m/z*: 454.0037, [M-H]⁻; accuracy: -5.5 ppm.

Figure S5. Full Mass Spectrum of compound **EMAC8000e**. Theoretical *m/z*: 404.0722, [M-H]⁻; accuracy: -5.4 ppm.

Figure S6. Full Mass Spectrum of compound **EMAC8000f**. Theoretical *m/z*: 431.0667, [M-H]⁻; accuracy: -5.3 ppm.
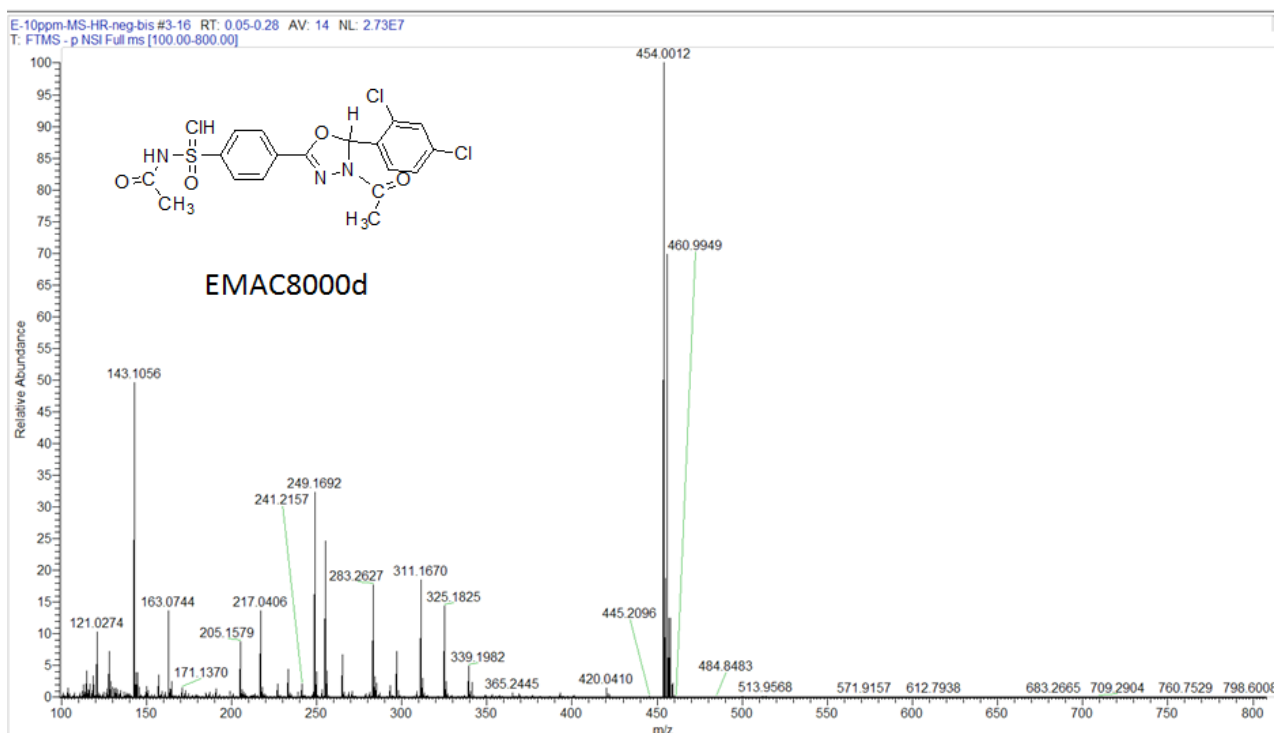
Figure S7. Full Mass Spectrum of compound **EMAC8000g**. Theoretical *m/z*: 431.0667, [M-H]⁻; accuracy: -5.3 ppm.

Figure S8. Full Mass Spectrum of compound **EMAC8000h**. Theoretical *m/z*: 416.0922, [M-H]⁻; accuracy: -5.0 ppm.

Figure S9. Full Mass Spectrum of compound **EMAC8000i**. Theoretical *m/z*: 431.0667, [M-H]⁻; accuracy: -5.3 ppm.
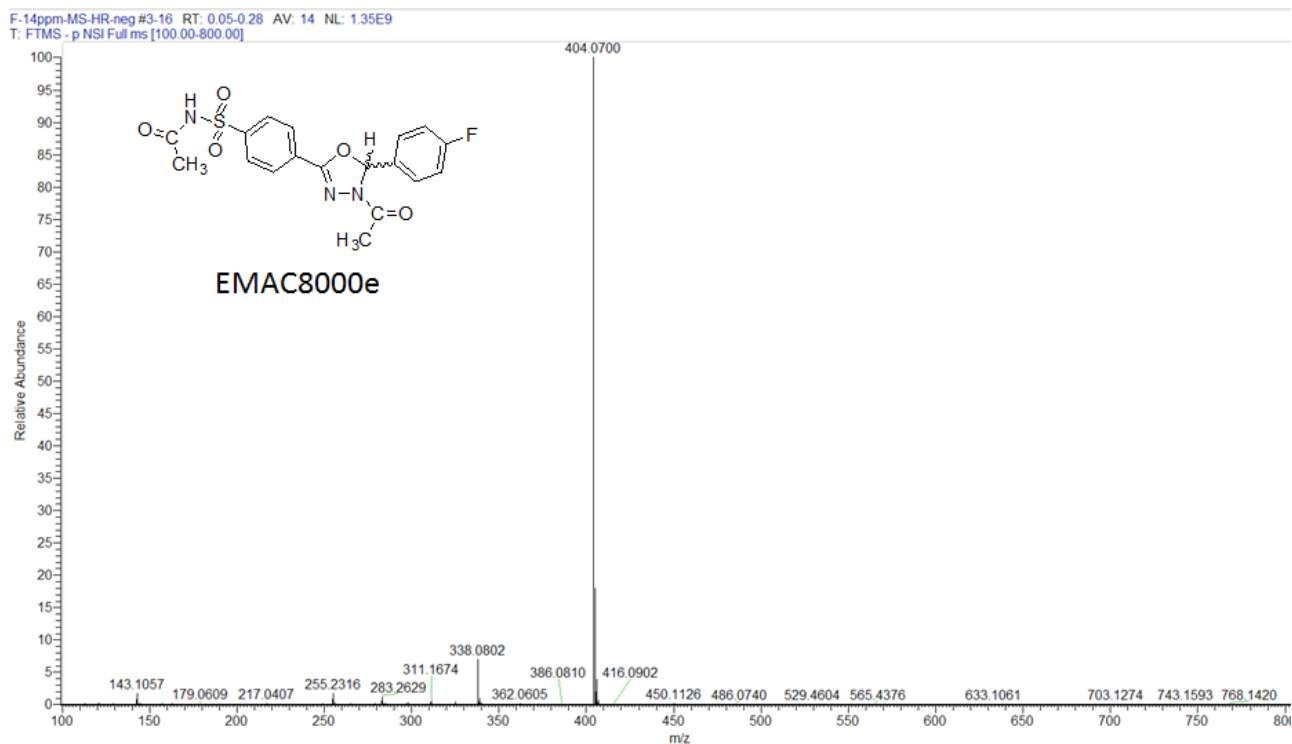

Figure S10. Full Mass Spectrum of compound **EMAC8000j**. Theoretical *m/z*: 400.0973, [M-H]⁻; accuracy: -5.5 ppm.
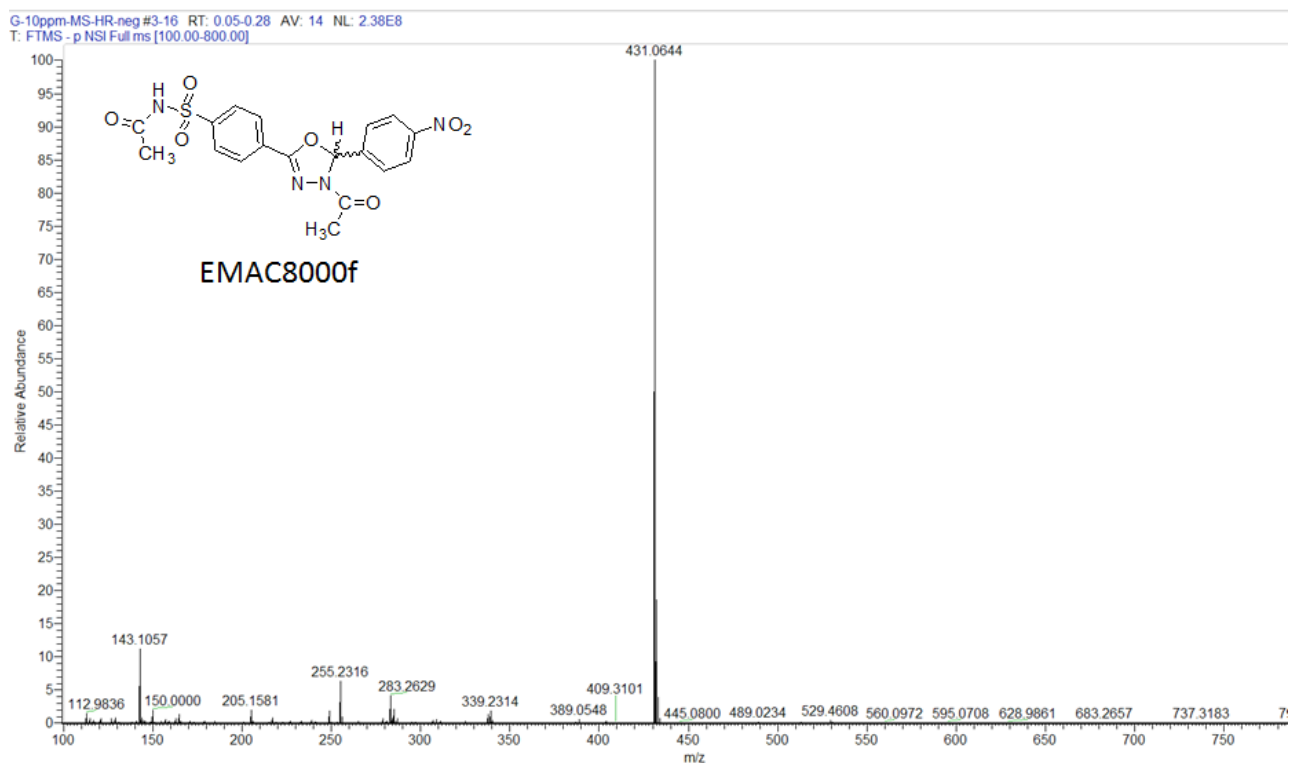
Figure S11. Full Mass Spectrum of compound **EMAC8000k**. Theoretical *m/z*: 416.0922, [M-H]⁻; accuracy: -5.3 ppm.
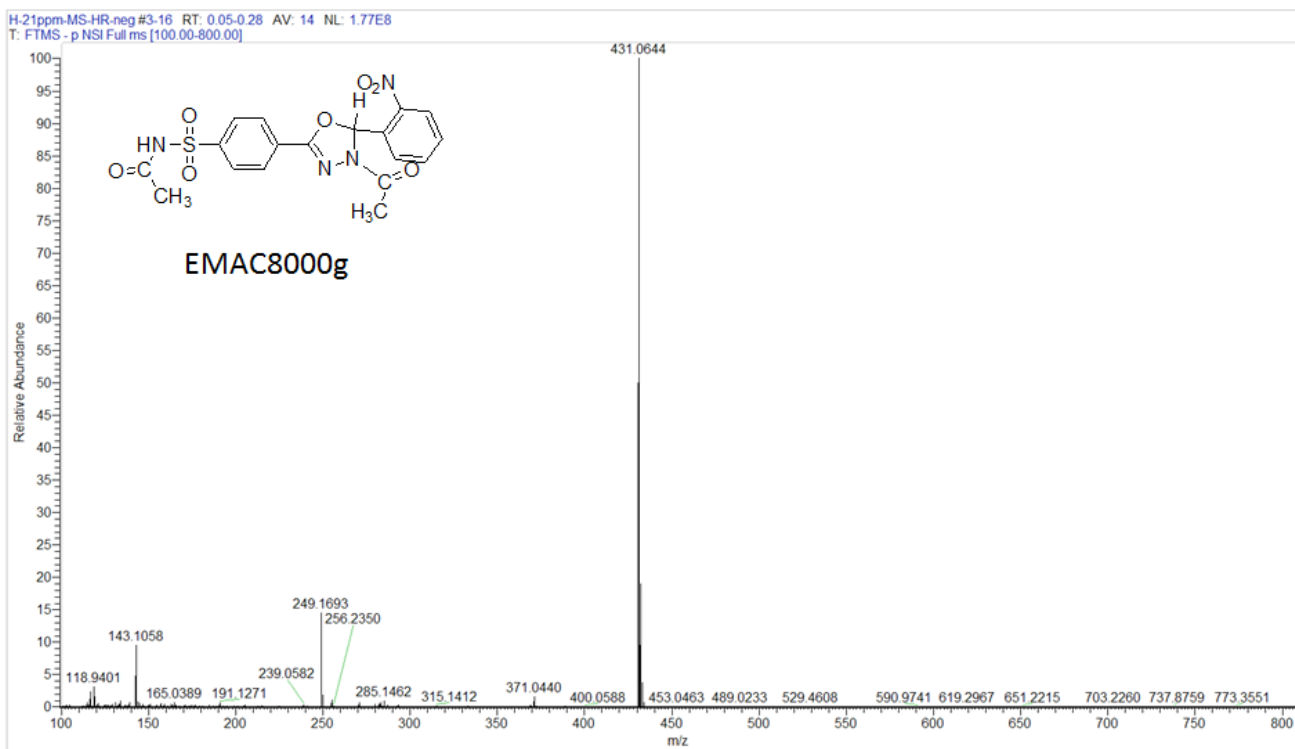

Figure S12. Full Mass Spectrum of compound **EMAC8000l**. Theoretical *m/z*: 422.0628, [M-H]⁻; accuracy: -5.2 ppm.

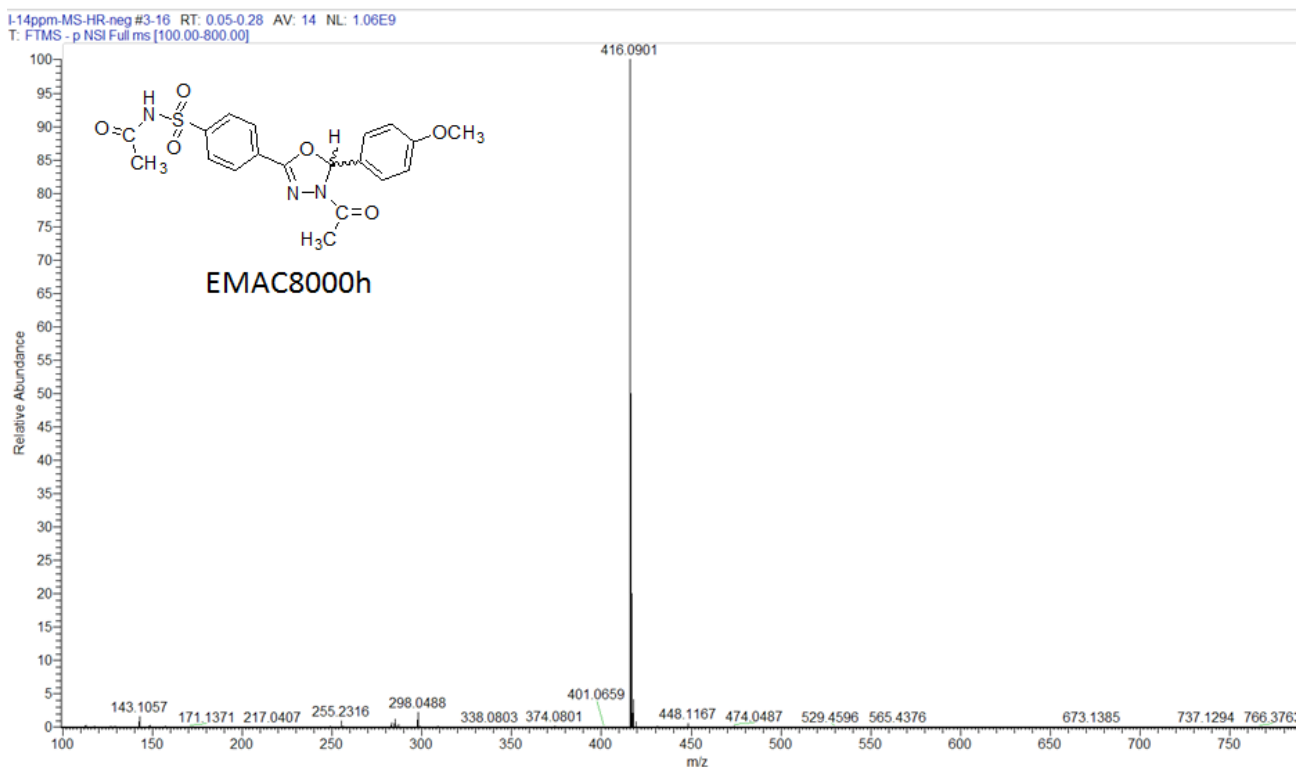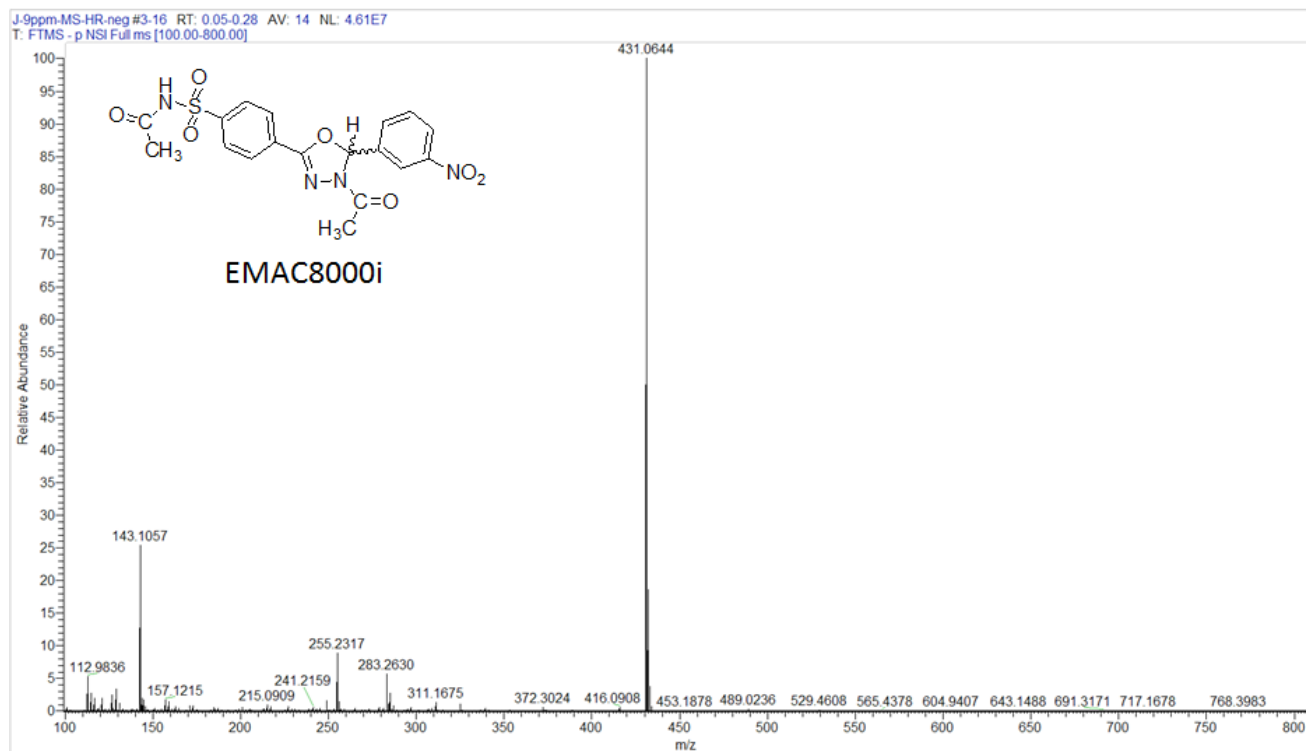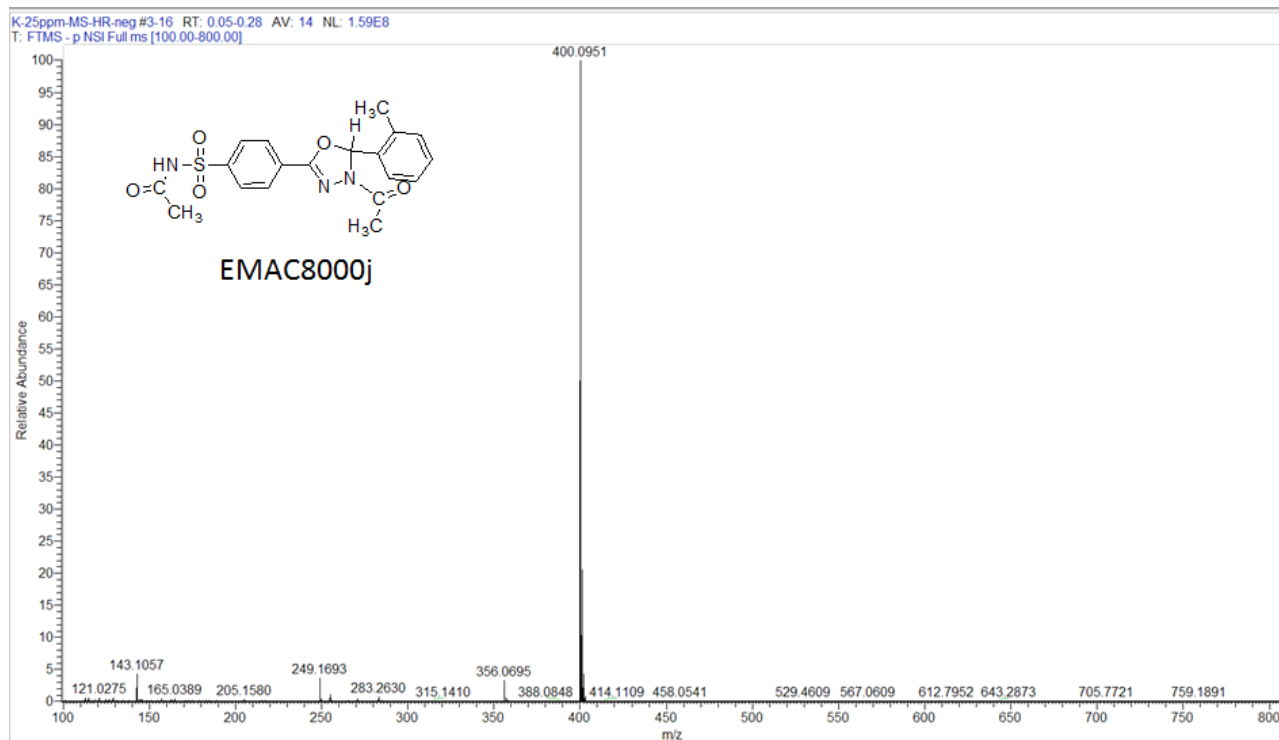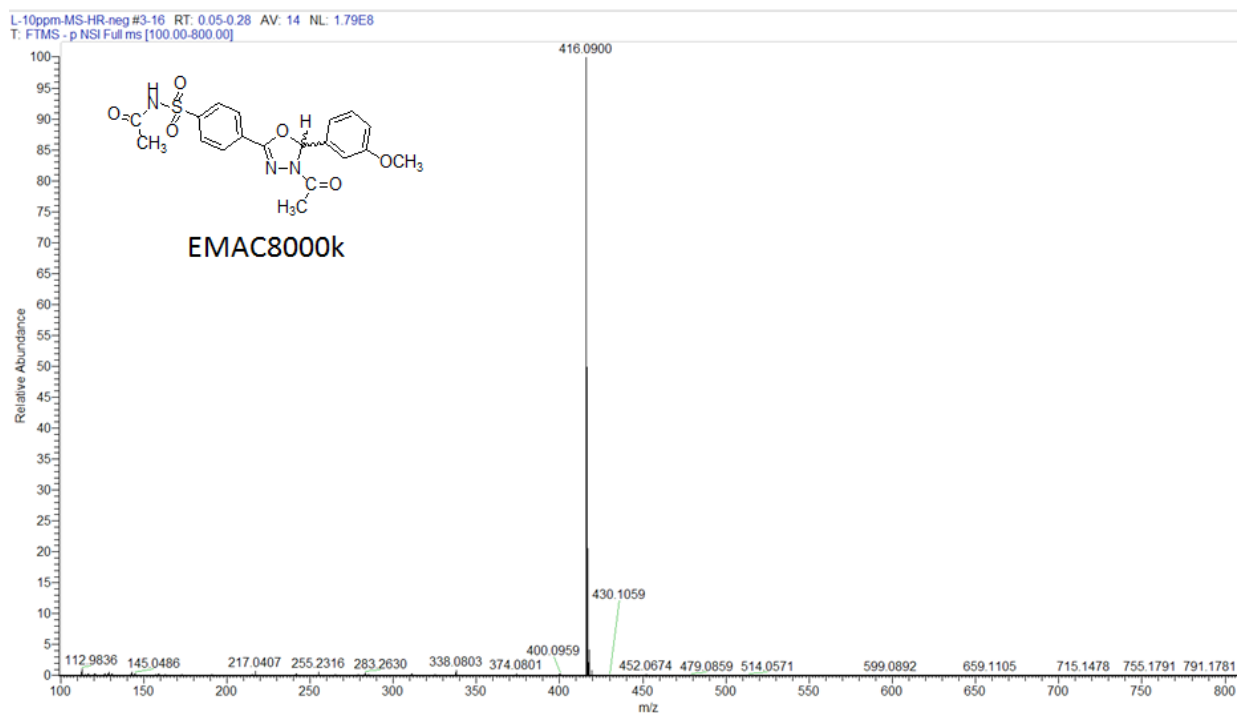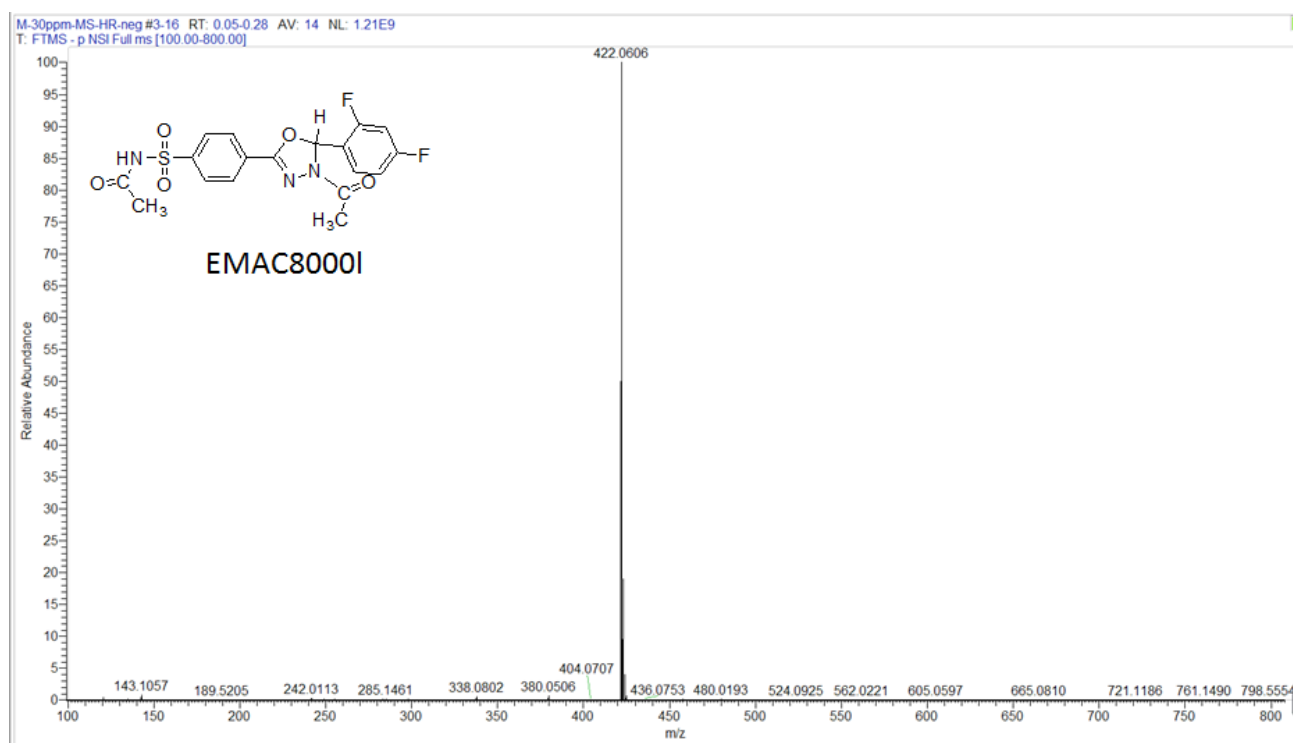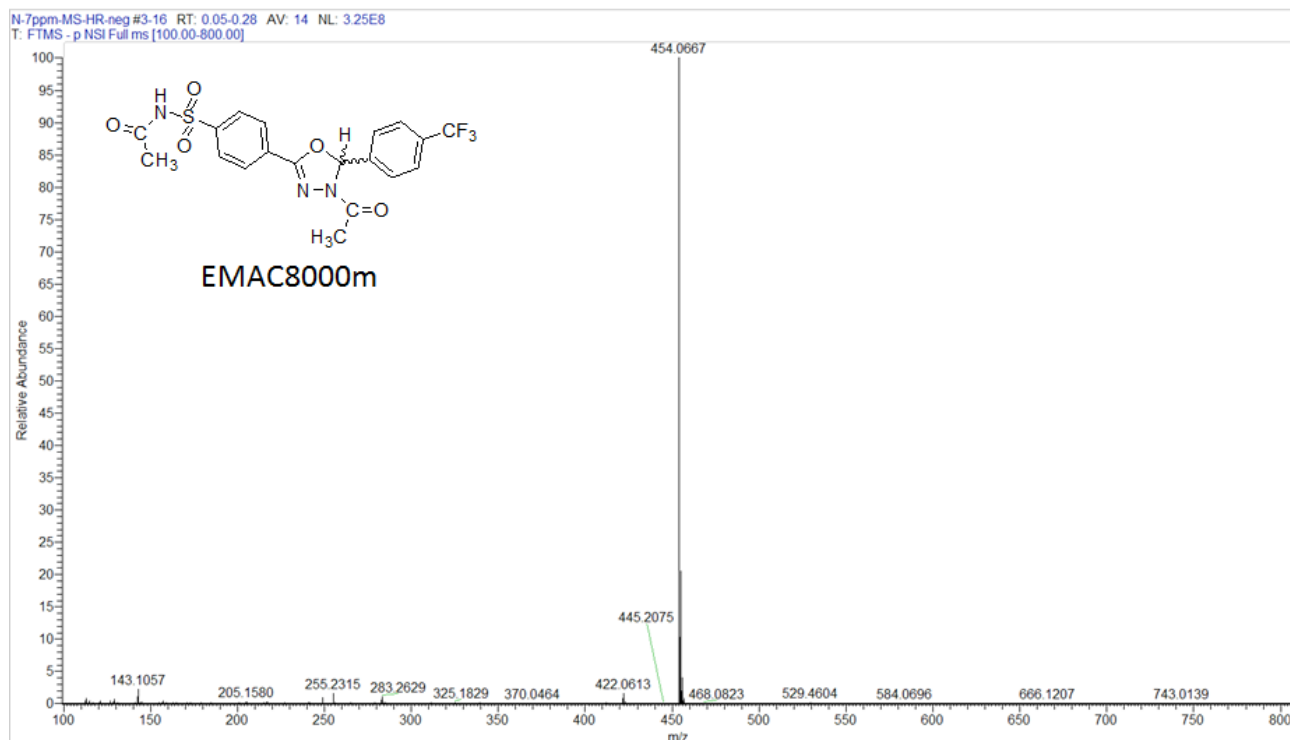**Figure S13.** Full Mass Spectrum of compound **EMAC8000m**. Theoretical *m/z*: 454.0690, [M-H]⁻; accuracy: -5.1 ppm.

Table S2. Theoretical and experimental *m/z* of compounds **EMAC8000 a-m**.

Compound	*Molecular formula*	*Exact mass*	*Theoretical [M-H]⁻*	*Experimental [M-H]⁻*	*Accuracy (ppm)*
EMAC8000a	$C_{18}H_{16}ClN_3O_5S$	421.0499	420.0426	420.0404	-5.2
EMAC8000b	$C_{19}H_{19}N_3O_5S$	401.1045	400.0973	400.0951	-5.5
EMAC8000c	$C_{19}H_{19}N_3O_6S$	417.0995	416.0922	416.0903	-4.6
EMAC8000d	$C_{18}H_{15}Cl_2N_3O_5S$	455.0110	454.0037	454.0012	-5.5
EMAC8000e	$C_{18}H_{16}FN_3O_5S$	405.0795	404.0722	404.0700	-5.4
EMAC8000f	$C_{18}H_{16}N_4O_7S$	432.0740	431.0667	431.0644	-5.3
EMAC8000g	$C_{18}H_{16}N_4O_7S$	432.0740	431.0667	431.0644	-5.3
EMAC8000h	$C_{19}H_{19}N_3O_6S$	417.0995	416.0922	416.0901	-5.0
EMAC8000i	$C_{18}H_{16}N_4O_7S$	432.0740	431.0667	431.0644	-5.3
EMAC8000j	$C_{19}H_{19}N_3O_5S$	401.1045	400.0973	400.0951	-5.5
EMAC8000k	$C_{19}H_{19}N_3O_6S$	417.0995	416.0922	416.0900	-5.3
EMAC8000l	$C_{18}H_{15}F_2N_3O_5S$	423.0701	422.0628	422.0606	-5.2
EMAC8000m	$C_{19}H_{16}F_3N_3O_5S$	455.0763	454.0690	454.0667	-5.1

Table S3. ^{1}H- ^{13}C-NMR chemical shifts of Compounds **EMAC8000a-m**.

Compound	^{1}H NMR and ^{13}C-NMR
EMAC8000a	^{1}H NMR (400 MHz, DMSO-d_6) δ(ppm): 7.82 (4H, cum, CH, Ar.), 7.51 (4H, m, CH, Ar.), 7.21 (1H, C_2H-oxadiaz.), 2.26 (3H, s, CH_3, $COCH_3$), 1.62 (3H, s, CH_3, $COCH_3$), NH not detected ^{13}C NMR (100 MHz, DMSO-d_6) δ(ppm): 176.38 (1C), 168.11 (1C), 155.56 (1C), 151.04 (1C), 136.80 (1C), 135.71 (1C), 130.11 (2C), 129.82 (2C), 128.70 (1C), 127.14 (2C), 125.75 (2C), 92.42 (1C), 27.98 (1C), 22.39 (1C)
EMA 8000b	^{1}H NMR (400 MHz, CDCl$_3$) δ(ppm): 8,53 (1H, bs, NH), 8.04 (2H, d, *J* 8.4, CH, Ar.), 7.97 (2H, d, *J* 8.4, CH, Ar.), 7.28 (2H, d, *J* 8, CH, Ar.), 7.14 (2H, d, *J* 8, CH, Ar.), 7.02 (1H, C_2H-oxadiaz.), 2.31 (3H, s, CH_3, $COCH_3$), 2.29 (3H, s, CH_3, CH_3-phenyl), 1.97 (3H, s, CH_3, $COCH_3$) ^{13}C NMR (100 MHz, CDCl$_3$) δ(ppm): 168.28 (1C), 167.84 (1C), 154.39 (1C), 140.98 (1C), 140.35 (1C), 133.13 (1C), 130.04 (1C), 129.85 (2C), 128.96 (2C), 127.52 (2C), 126.57 (2C), 93.57 (1C), 23.68 (1C), 21.64 (1C), 21.44 (1C)
EMAC8000c	^{1}H NMR (400 MHz, CDCl$_3$) δ(ppm): 8.023 (2H, d, *J* 8.4, CH, Ar.), 7.96 (2H, d, *J* 8.4, CH, Ar.), 7.31 (2H, m), 7.22 (1H, m), 6.89 (2H, m), 3.77 (3H, s, CH_3, 4-OCH_3- phenyl), 2.31 (3H, s, CH_3, $COCH_3$), 1.98 (3H, s, CH_3, $COCH_3$), NH not detected ^{13}C NMR (100 MHz, CDCl$_3$) δ(ppm): 167.63 (1C), 160.73 (1C), 157.87 (1C), 144.20 (1C), 140.56 (1C), 131.85 (1C), 130.65 (1C), 128.89 (2C), 128.35 (1C), 127.52 (2C), 123.58 (1C), 120.91 (1C), 111.62 (1C), 90.71 (1C), 55.92 (1C), 23.62 (1C), 21.35 (1C)
EMAC8000d	^{1}H NMR (400 MHz, CDCl$_3$) δ(ppm): 8.25 (1H, bs, NH), 8.05 (2H, d, *J* 8.8, CH, Ar.), 7,95 (2H, d, *J* 8.8, CH, Ar.), 7.41 (1H, s, CH, Ar.), 7.25 (3H, m, CH, Ar., and C_2H-oxadiaz.), 2.33 (3H, s, CH_3, $COCH_3$), 1.99 (3H, s, CH_3, $COCH_3$) ^{13}C NMR (400 MHz, CDCl$_3$) δ(ppm): 172.46 (1C), 171.75 (1C), 169.71 (1C), 158.69 (1C), 147.67 (1C), 134.54 (1C), 133.13 (1C), 131.29 (1C), 130.58 (1C), 129.68 (1C), 129.74 (1C), 128.96 (2C), 127.86 (1C), 127.56 (2C), 90.95 (1C), 23.68 (1C), 21.46 (1C)
EMAC8000e	^{1}H NMR (400 MHz, DMSO-d_6) δ(ppm): 12.23 (1H, bs, NH), 8.02 (4H, cum, CH, Ar.), 7.54 (2H, m, CH, Ar.), 7.25 (3H, m, CH Ar. and C_2H-oxadiaz.), 2.25 (3H, s, CH_3, $COCH_3$), 1.91 (3H, s, CH_3, $COCH_3$) ^{13}C NMR (100 MHz, DMSO-d_6) δ(ppm): 170.18 (1C), 168.28 (1C), 154.59 (1C), 142.95 (1C), 134.02 (1C), 133.99 (1C), 130.42 (1C), 130.34 (1C), 129.74 (1C), 129.55 (2C), 128.48 (2C), 117.10 (1C), 116.88 (1C), 93.11 (1C), 24.62 (1C), 22.36 (1C)
EMAC8000f	^{1}H NMR (400 MHz, DMSO-d_6) δ(ppm): 12.24 (1H, bs, NH), 8.28 (2H, d, *J* 8.8, CH, Ar.), 8.04 (4H, cum, CH, Ar.), 7.79 (2H, d, *J* 8.8, CH, Ar.), 7.37 (1H, C_2H-oxadiaz.), 2.27 (3H, s, CH_3, $COCH_3$), 1.91 (3H, s, CH_3, $COCH_3$) ^{13}C NMR (400 MHz, DMSO-d_6) δ(ppm): 170.24 (1C), 168.55 (1C), 154.79 (1C), 149.65 (1C), 143.88 (1C), 143.14 (1C), 129.58 (4C), 129.47 (1C), 128.56 (2C), 125.27 (2C), 92.43 (1C), 24.50 (1C), 22.41 (1C)

EMAC8000g	^{1}H NMR (400 MHz, DMSO-d_6) δ(ppm): 12.23 (1H, bs, NH), 8.076 (1H, d, *Jo* 8, *Jm 0.8*, CH, Ar.), 8.01 (4H, cum, CH, Ar.), 7.79 (1H, t, *Jo 7.6*, *Jm 0.8*, CH, Ar.), 7,71 (1H, t, *Jo* 8, *Jm 0.8* /1.2, CH, Ar.), 7,65 (1H, d, *Jo* 8, *Jm 0.8*, CH, Ar.), 7.60 (1H, C$_2$H-oxadiaz.), 2.26 (3H, s, CH$_3$, COCH$_3$), 1.90 (3H, s, CH$_3$, COCH$_3$) ^{13}C NMR (100 MHz, DMSO-d_6) δ(ppm): 170.17 (2C), 154.65 (1C), 149.27 (1C), 143.03 (1C), 135.52 (1C), 132.80 (1C), 130.59 (1C), 129.91 (1C), 129.59 (2C), 129.50 (1C), 128. 51 (2C), 126.12 (1C), 89.85 (1C), 24.45 (1C), 22.28 (1C)
EMAC8000h	^{1}H NMR (400 MHz, DMSO-d_6) δ(ppm): 12.22 (1H, bs, NH), 8.01 (4H, cum, CH, Ar.), 7.39 (2H, d, *J* 8.8, CH, Ar.), 7.15 (1H, C$_2$H-oxadiaz.),6.95 (2H, d, *J* 8, CH, Ar.), 3.74 (3H, s, CH$_3$, 4-OCH$_3$- phenyl), 2.24 (3H, s, CH$_3$, COCH$_3$), 1.90 (3H, s, CH$_3$, COCH$_3$) ^{13}C NMR (100 MHz, DMSO-d_6) δ(ppm): 170.31 (1C), 168.10 (1C), 161.68 (1C), 154.58 (1C), 142.97 (1C), 129.84 (1C), 129.74 (1C), 129.53 (2C), 129.42 (2C), 128.40 (2C), 115.38 (2C), 93.78 (1C), 56.50 (1C), 24.51 (1C), 22.49 (1C)
EMAC8000i	^{1}H NMR (400 MHz, DMSO-d_6) δ(ppm): 12.24 (1H, bs, NH), 8.35 (1H, m, CH, Ar.), 8.28 (1H, m, CH, Ar.), 8.03 (4H, cum, CH, Ar.), 7.96 (1H, m, CH, Ar.), 7,73 (1H, t, *J* 8, CH, Ar), 7.40 (1H, C$_2$H-oxadiaz.), 2.28 (3H, s, CH$_3$, COCH$_3$), 1.91 (3H, s, CH$_3$, COCH$_3$) ^{13}C NMR (100 MHz, DMSO-d_6) δ(ppm): 170.18 (1C), 168.66 (1C), 154.73 (1C), 149.19 (1C), 143.05 (1C), 139.48 (1C), 134.44 (1C), 131.98 (1C), 129.57 (2C), 129.55 (1C), 128.58 (2C), 126.11 (1C), 123.06 (1C), 92.48 (1C), 24.47 (1C), 22.45 (1C)
EMAC8000j	^{1}H NMR (400 MHz, CDCl$_3$) δ(ppm): 8.39 (1H, bs, NH), 8.03 (2H, d, *J* 8.8, CH, Ar.), 7.95 (2H, d, *J* 8.8, CH, Ar.), 7.19 (5H, m, CH, Ar. and C$_2$H-oxadiaz.), 2.47 (3H, s, CH$_3$, 2-CH$_3$-phenyl), 2.35 (3H, s, CH$_3$, COCH$_3$), 1.96 (3H, s, CH$_3$, COCH$_3$) ^{13}C NMR (100 MHz, CDCl$_3$) δ(ppm): 168.21 (1C), 167.65 (1C), 154.20 (1C), 140.97 (1C), 136.80 (1C), 133.35 (1C), 131.33 (1C), 130.31 (1C), 130.10 (1C), 128.89 (2C), 127.53 (2C), 126.68 (1C), 126.52 (1C), 91.80 (1C), 23.67 (1C), 23.60 (1C), 21.66 (1C)
EMAC8000k	^{1}H NMR (400 MHz, DMSO-d_6) δ(ppm): 12.22 (1H, bs, NH), 8.01 (4H, cum, CH, Ar.), 7.33 (1H, t, *J* 8.0, CH, Ar.), 7.17 (1H, s, C$_2$H-oxadiaz.), 6.99 (3H, m, CH, Ar.), 3.74 (3H, s, CH$_3$, 4-OCH$_3$-phenyl), 2.26 (3H, s, CH$_3$, COCH$_3$), 1.91 (3H, s, CH$_3$, COCH$_3$) ^{13}C NMR (100 MHz, DMSO-d_6) δ(ppm): 170.18 (1C), 168.25 (1C), 160.69 (1C), 154.65 (1C), 142.92 (1C), 139.05 (1C), 131.37 (1C), 129.76 (1C), 129.56 (2C), 128.47 (2C), 119.71 (1C), 116.51 (1C), 113.69 (1C), 93.64 (1C), 56.47 (1C), 24.47 (1C), 22.48 (1C)
EMAC8000l	^{1}H NMR (400 MHz, CDCl$_3$) δ(ppm): δH 8.56 (1H, bs, NH), 8.05 (2H, d, *J* 8.8, CH, Ar.), 7.96 (2H, d, *J* 8.8, CH, Ar.), 7.31 (1H, dd, *J* 8.4, CH, Ar.), 7.16 (1H, s, C$_2$H-oxadiaz.), 6.82 (2H, m, CH, Ar.), 2.32 (3H, s, CH$_3$, COCH$_3$), 1.99 (3H, s, CH$_3$, COCH$_3$) ^{13}C NMR (400 MHz, CDCl$_3$) δ(ppm): 168.24 (1C), 167.89 (1C), 163.15 (1C), 160.12 (1C), 154.24 (1C), 141.10 (1C), 130.19 (1C), 129.79 (1C), 128.94 (2C), 127.55 (2C), 119.50 (1C), 111.88 (1C),105.04 (1C), 89.21 (1C), 23.69 (1C), 21.53 (1C)

EMAC8000m	^{1}H NMR (400 MHz, DMSO-d$_6$) δ(ppm): 7.80 (6H, m, CH, Ar.), 7.70 (2H, d, CH, Ar.) 7.28 (1H, s, CH, C$_2$H-oxadiaz.), 2.25 (3H, s, CH$_3$, COCH$_3$), 1.61 (3H, s, CH$_3$, COCH$_3$), NH not detected ^{13}C NMR (100 MHz, DMSO-d$_6$) δ(ppm): 176.40 (1C), 168.24 (1C), 155.65 (1C), 151.08 (1C), 142.02 (1C), 131.25 (1C), 128.87 (2C), 128.70 (2C), 127.20 (2C), 127.09 (2C), 125.66 (1C), 92.25 (1C), 41.06 (1C), 27.97 (1C), 22.42 (1C)

^{1}H NMR spectra of compounds EMAC8000a-m:
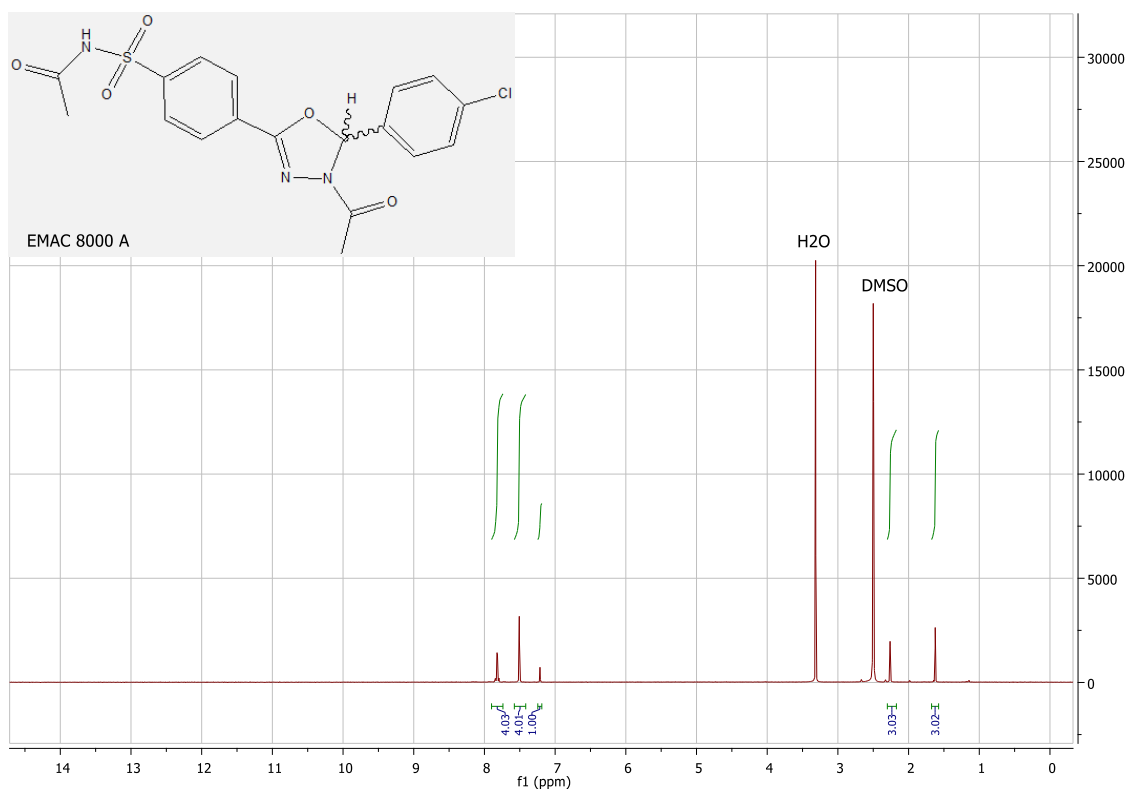
Figure S14. ^{1}H NMR spectrum (400 MHz, DMSO-d$_6$) of **EMAC8000a**.
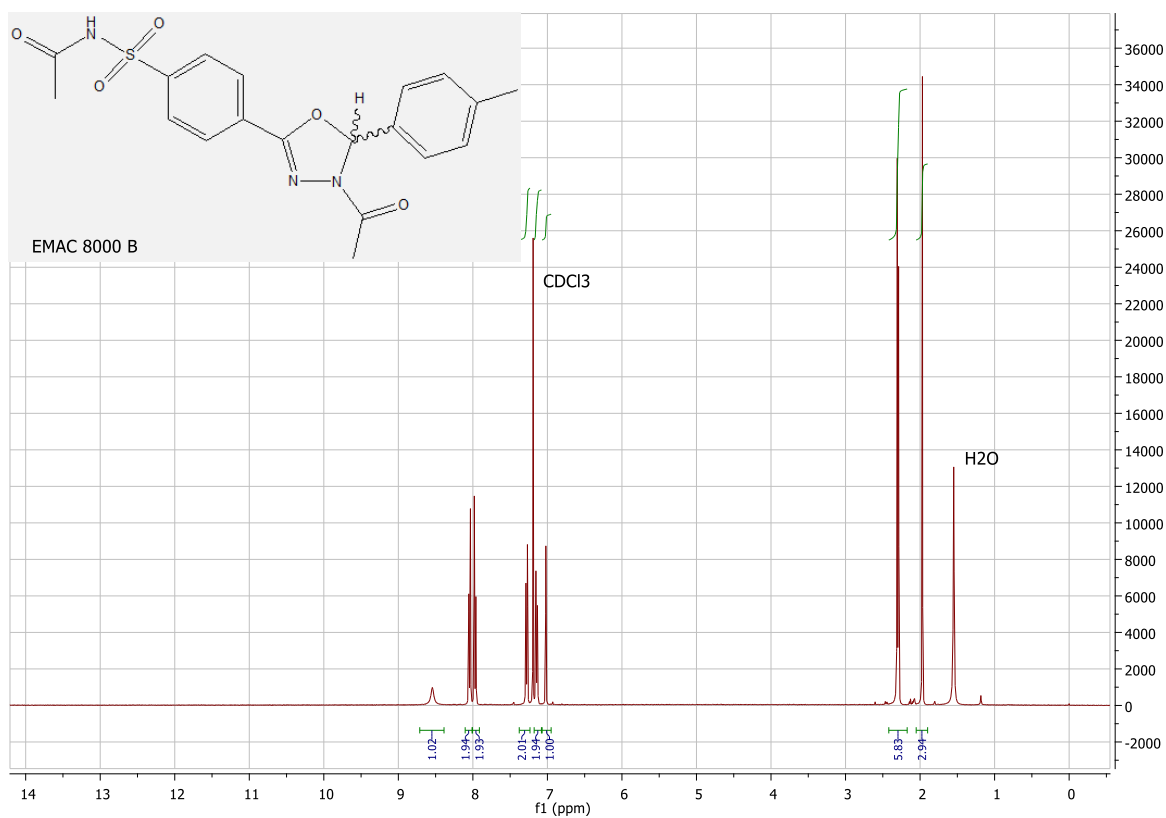
Figure S15. ^{1}H NMR spectrum (400 MHz, CDCl$_3$) of **EMAC8000b**.
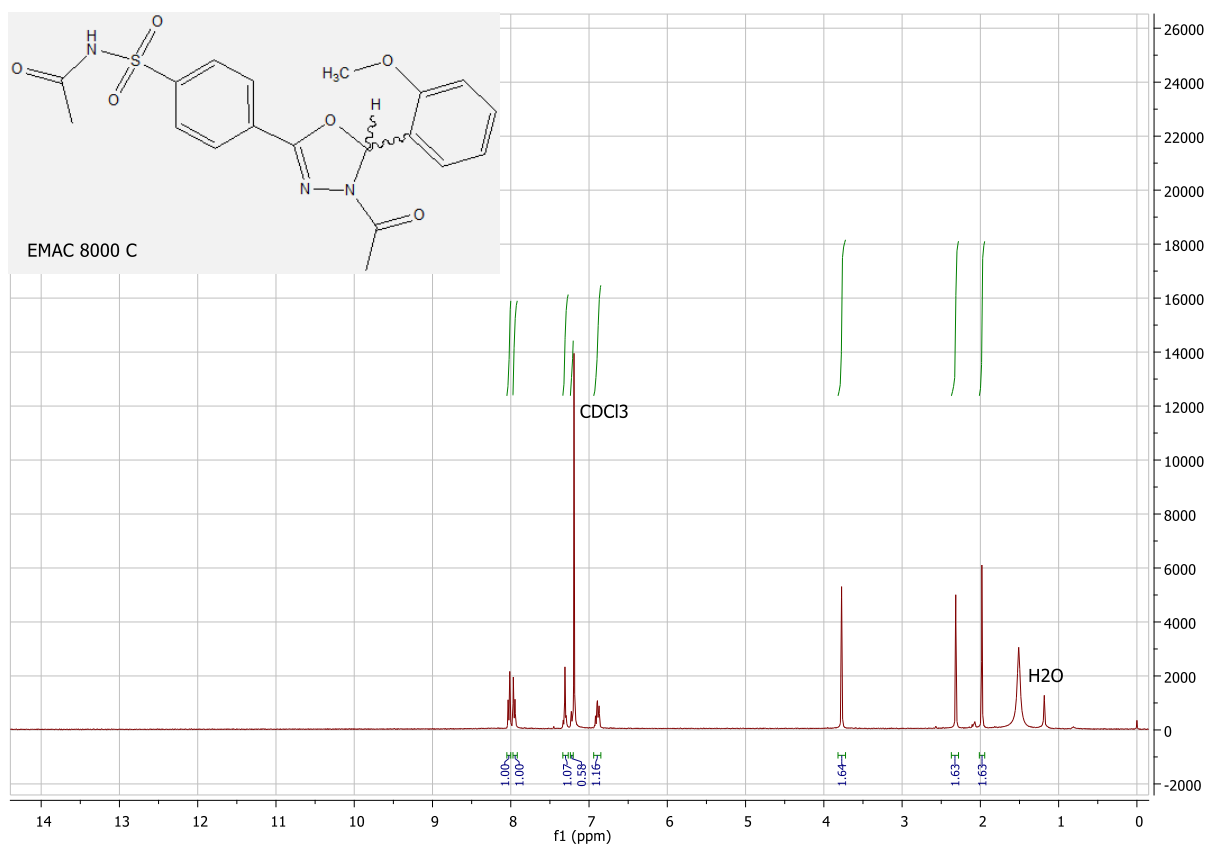
Figure S16. ^{1}H NMR spectrum (400 MHz, CDCl$_3$) of **EMAC8000c**.
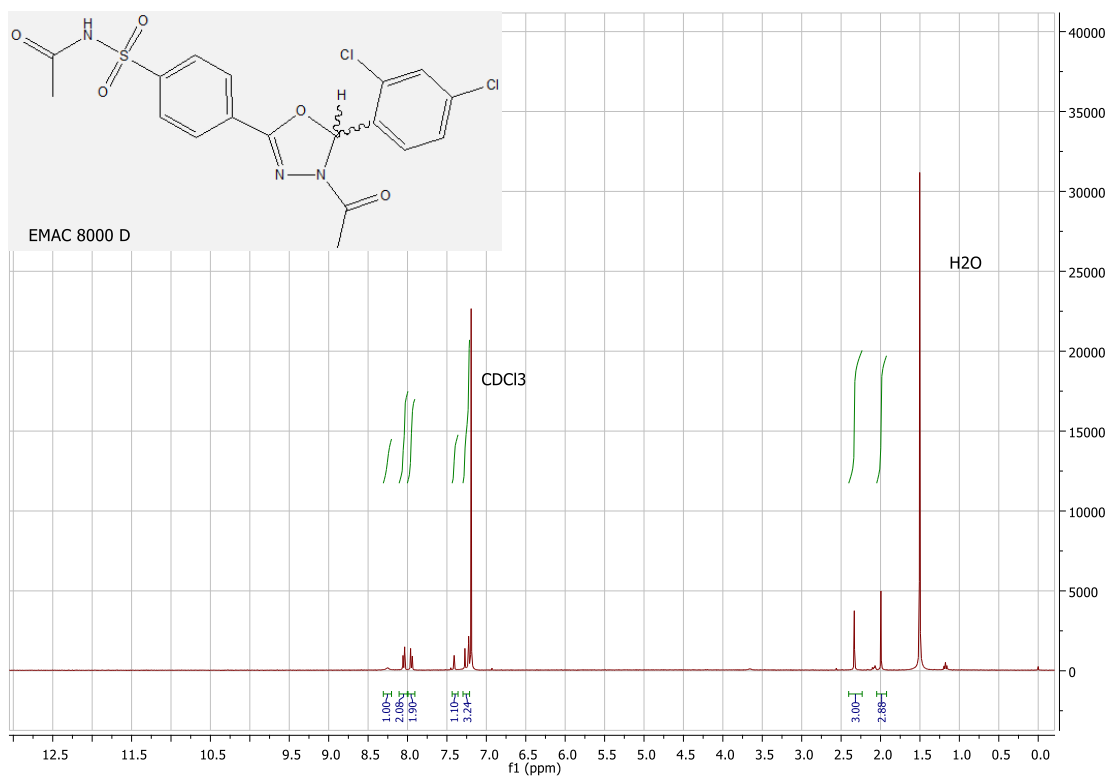
Figure S17. ^{1}H NMR spectrum (400 MHz, CDCl$_3$) of **EMAC8000d**.
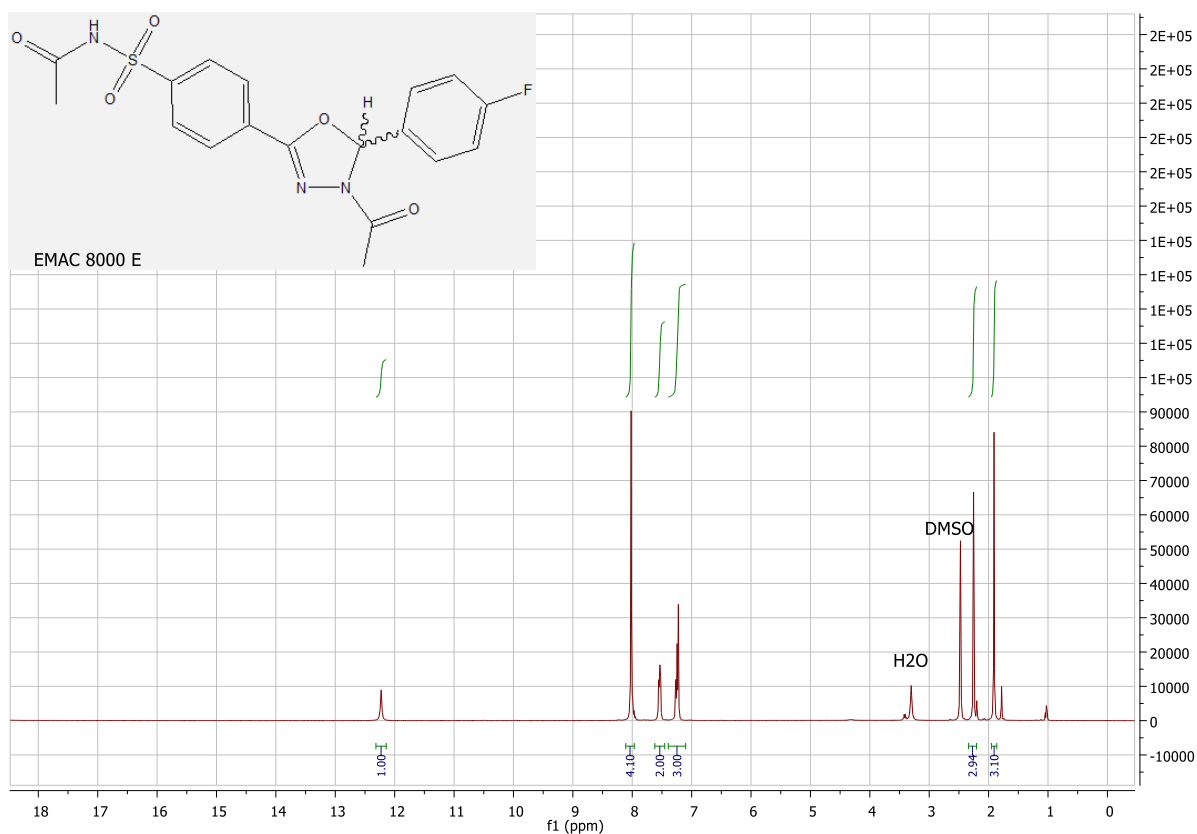
Figure S18. ^{1}H NMR spectrum (400 MHz, DMSO-d$_6$) of **EMAC8000e**.
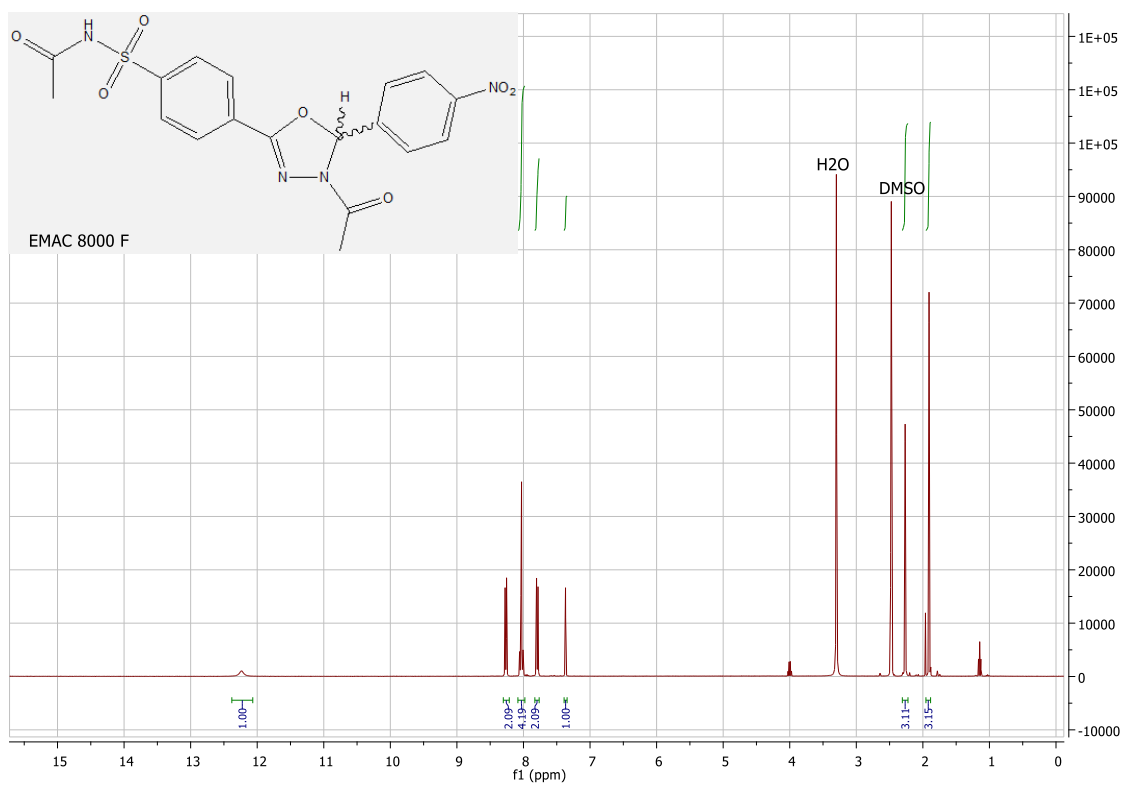
Figure S19. ^{1}H NMR spectrum (400 MHz, DMSO-d$_6$) of **EMAC8000f**.

16
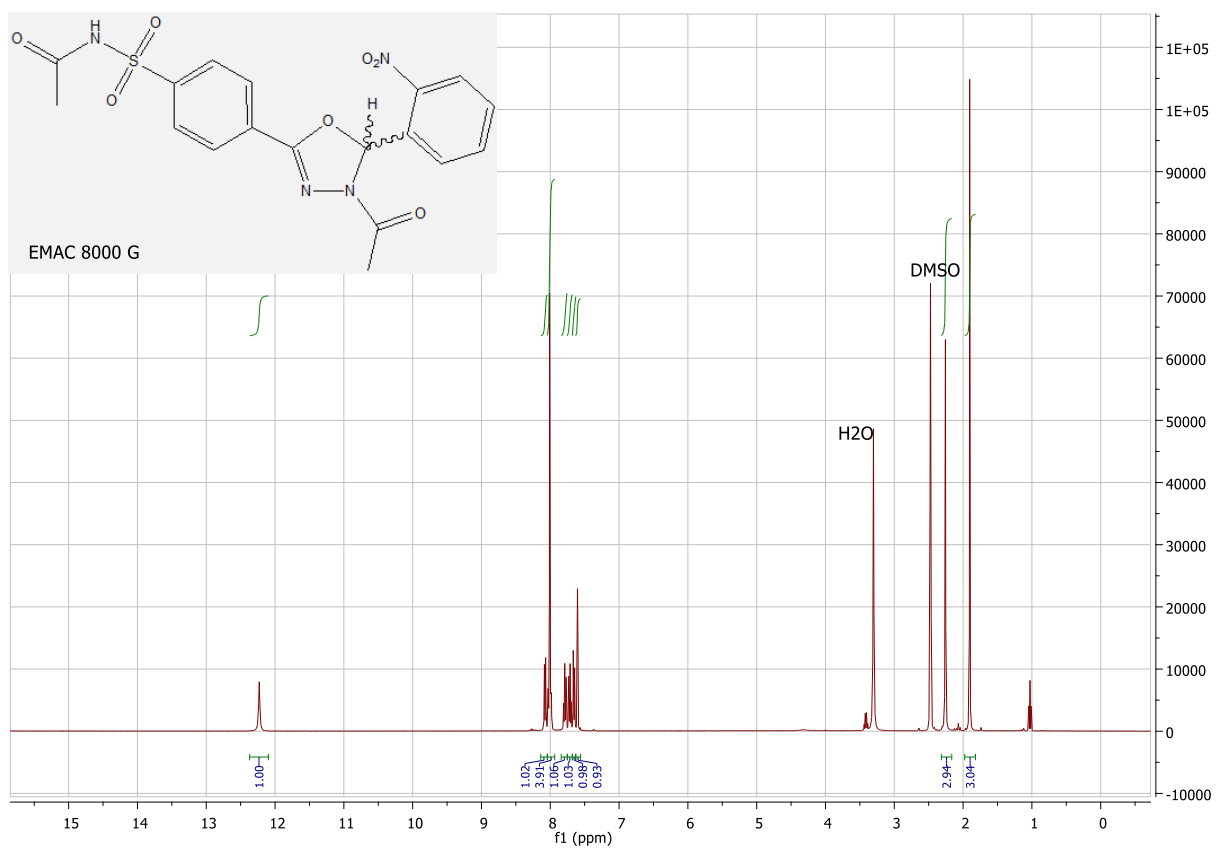
Figure S20. ^{1}H NMR spectrum (400 MHz, DMSO-d$_6$) of **EMAC8000g**.
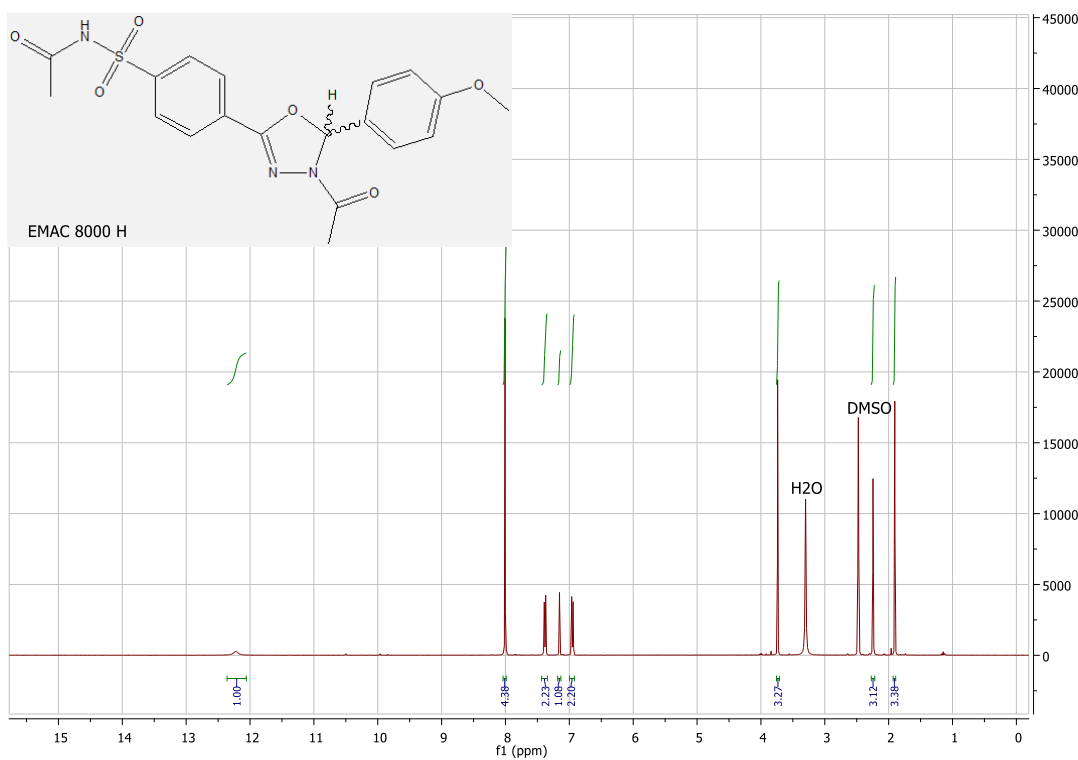
Figure S21. ^{1}H NMR spectrum (400 MHz, DMSO-d$_6$) of **EMAC8000h**.
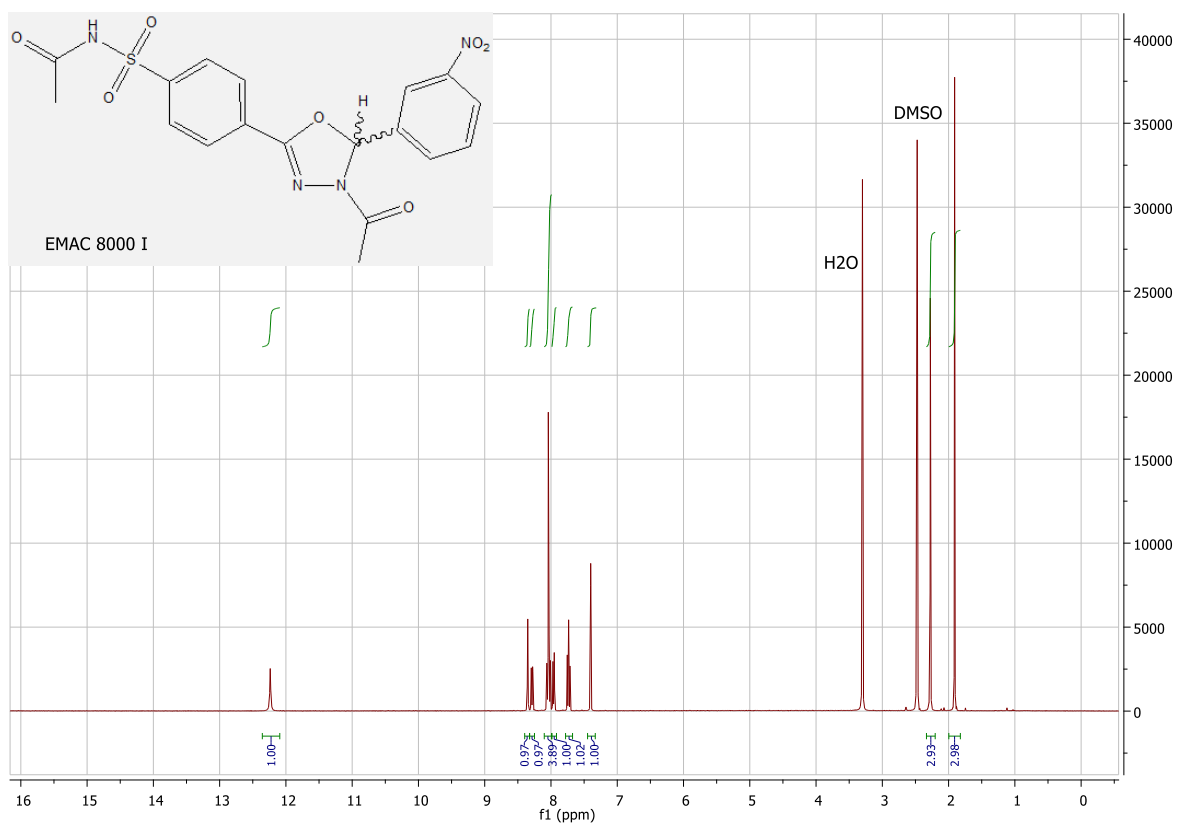
Figure S22. ^{1}H NMR spectrum (400 MHz, DMSO-d$_6$) of **EMAC8000i**.
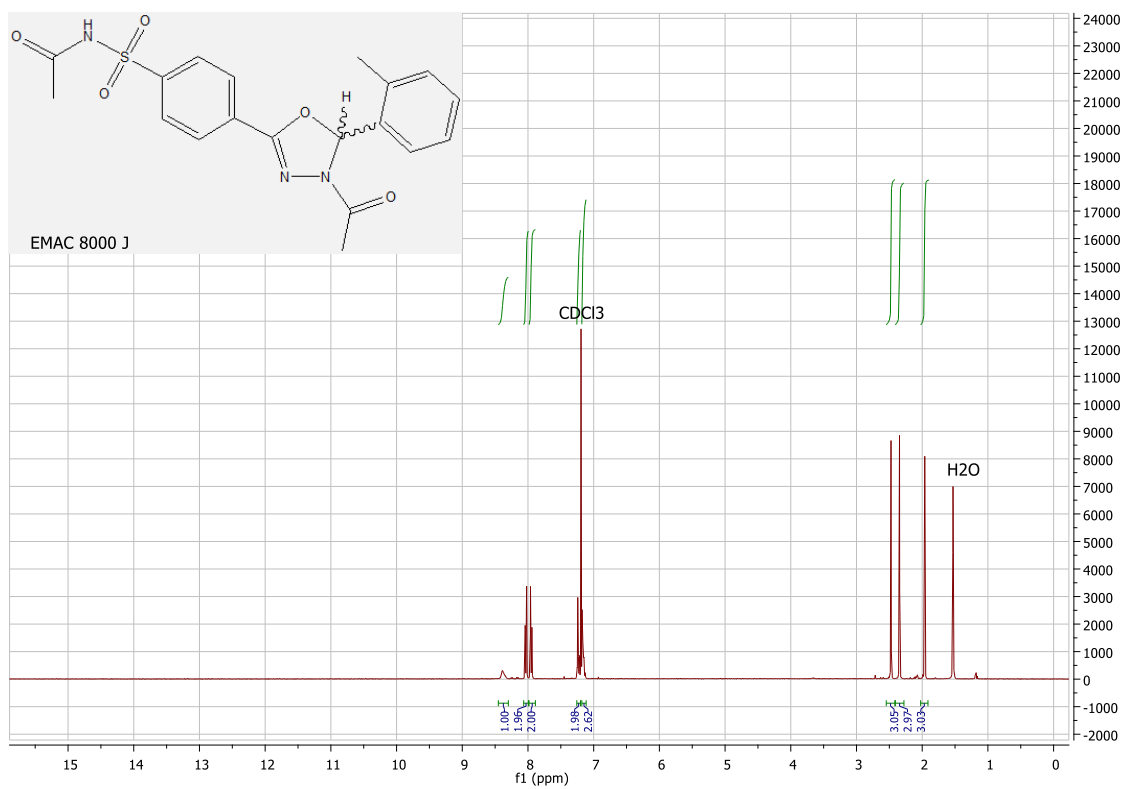
Figure S23. ^{1}H NMR spectrum (400 MHz, CDCl$_3$) of **EMAC8000j**.
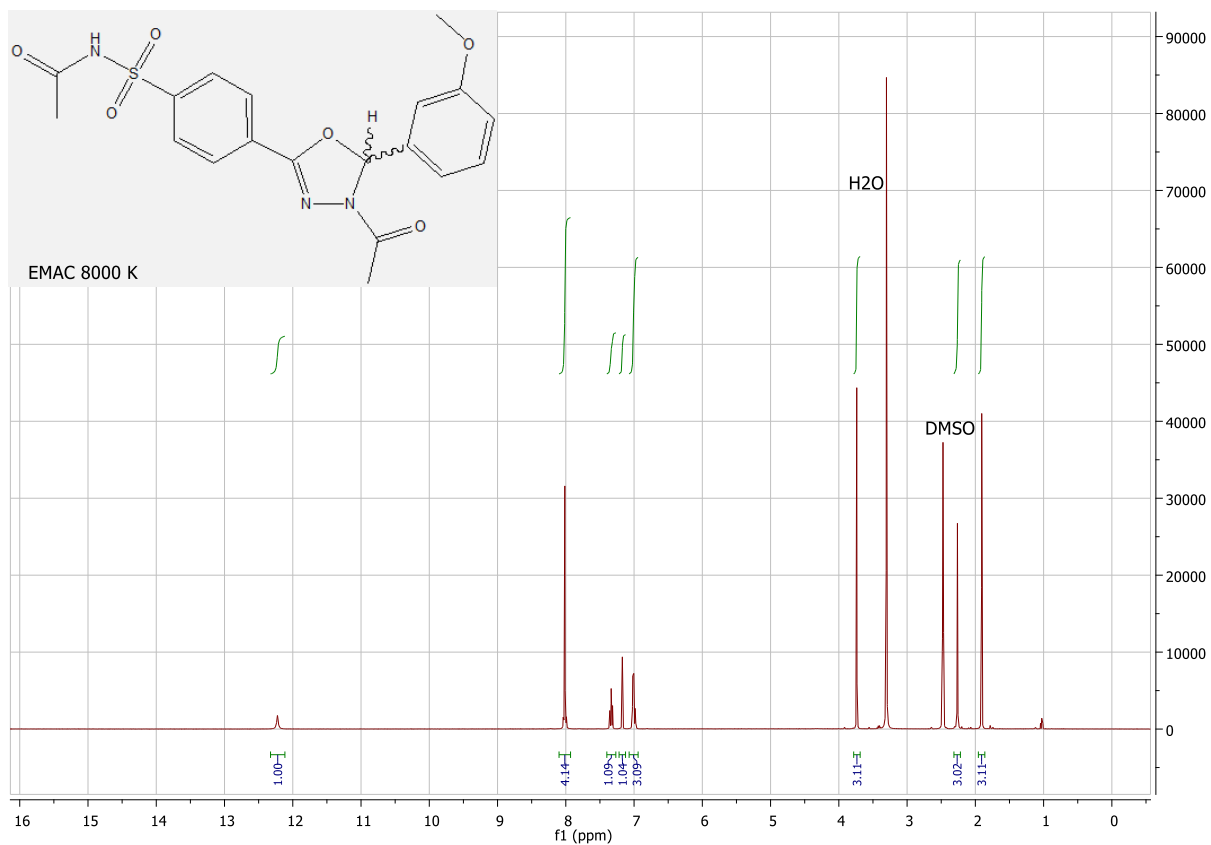
Figure S24. ^{1}H NMR spectrum (400 MHz DMSO-d$_6$) of **EMAC8000k**.
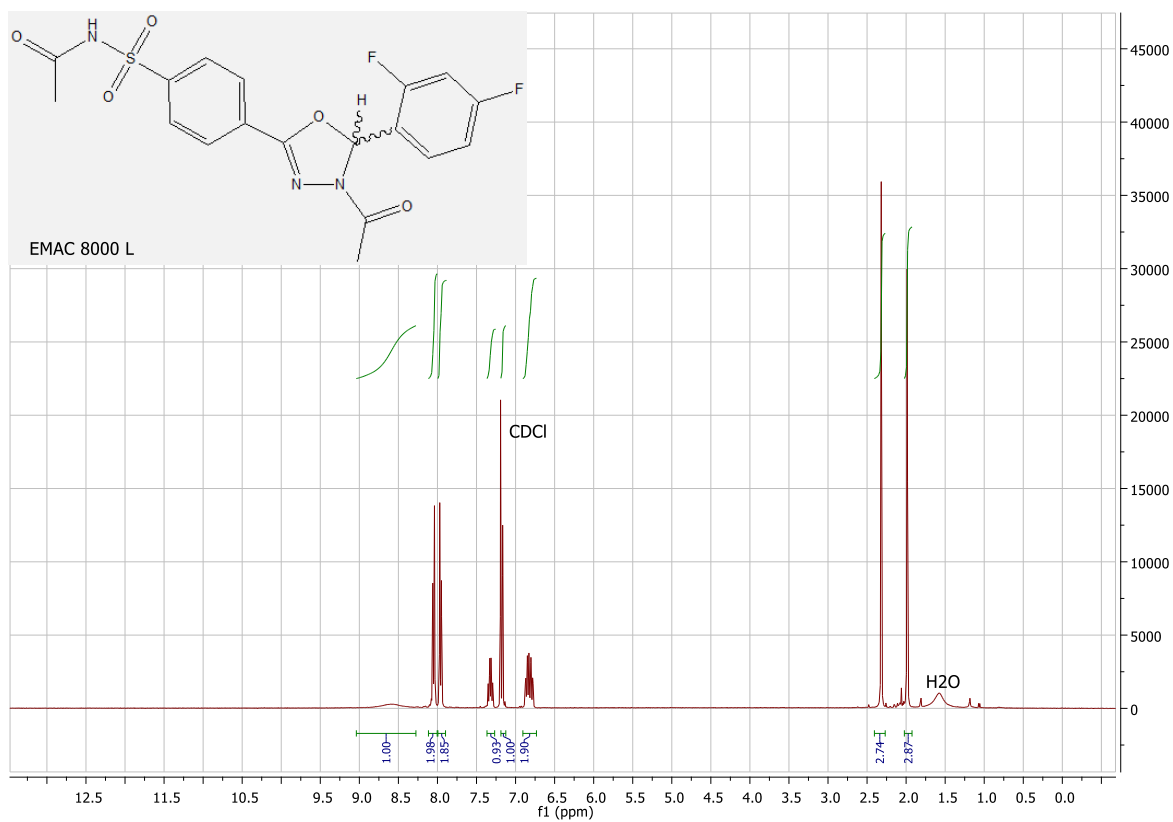
Figure S25. ^{1}H NMR spectrum (400 MHz CDCl$_3$) of **EMAC8000l**.
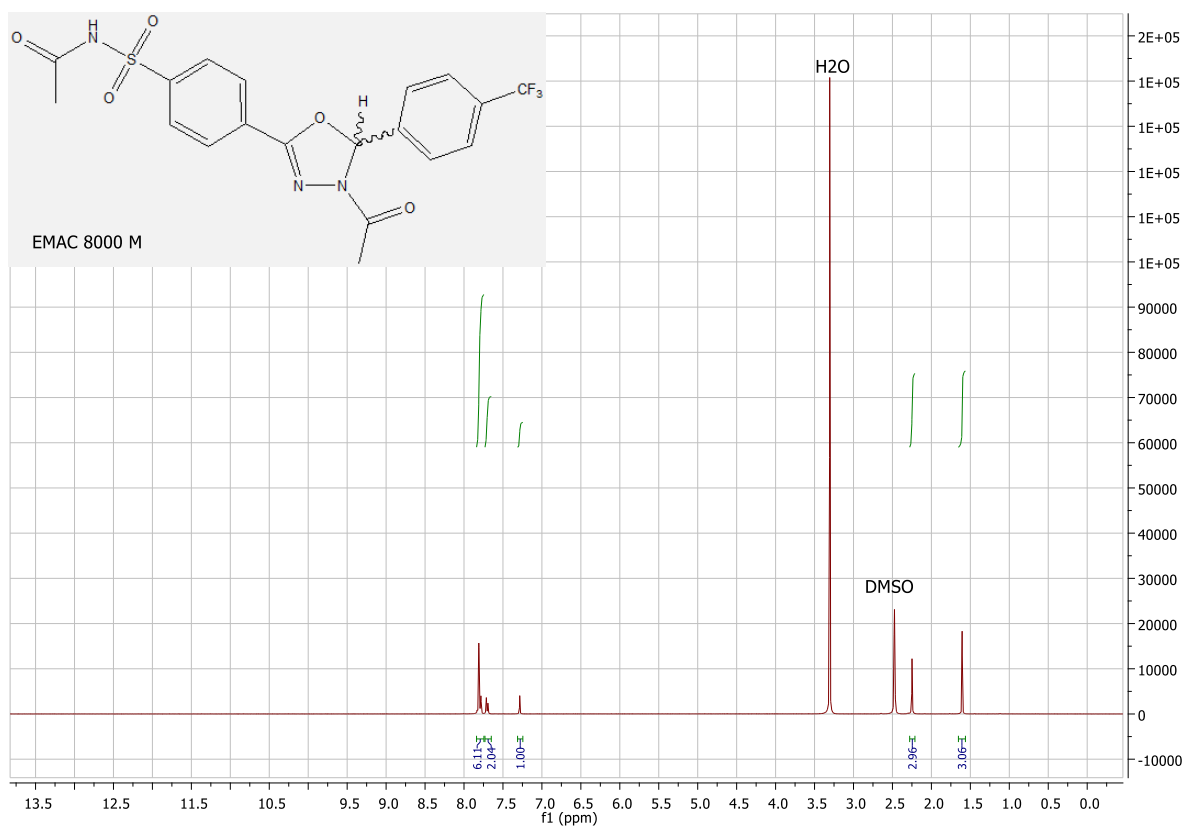
Figure S26. ^{1}H NMR spectrum (400 MHz DMSO-d$_6$) of **EMAC8000m**.

HPLC analysis of the tested compounds

The purity of the tested compounds was checked by HPLC before performing the biological assays. Compounds **EMAC8000a-m** were monitored with the same instrument mentioned in the general part, equipped with a 250 x 4.6 mm Polaris C-18-A column, particle size 5 μm (Varian), using as eluents ACN/H$_2$O (7:3, flow 1 mL/min. Purity of all compounds was ≥ 95%.

HPLC enantioseparation

In analytical enantioseparation (Chiralpak IA column: 250 x 4.6 mm I.D.) standard solutions was prepared by dissolving about 1 mg of sample into 10 mL of ethanol-acetonitrile 60-40 (v/v) mixture. The injection volume was 50 μL. In semipreparative enantioseparation (Chiralpak IA column: 250 x 10 mm I.D.) standard solutions was prepared by dissolving about 4 mg of sample into 1 mL of ethanol-acetonitrile/H$_2$O 60-40 (v/v) mixture. The injection volume was 500 μL.

The best chromatographic discrimination for compound **EMAC8000d** was obtained with ethanol-acetonitrile/H$_2$O 55-40-5 (v/v/v) mixture on the 1-cm I.D. IA column (Figure S27).
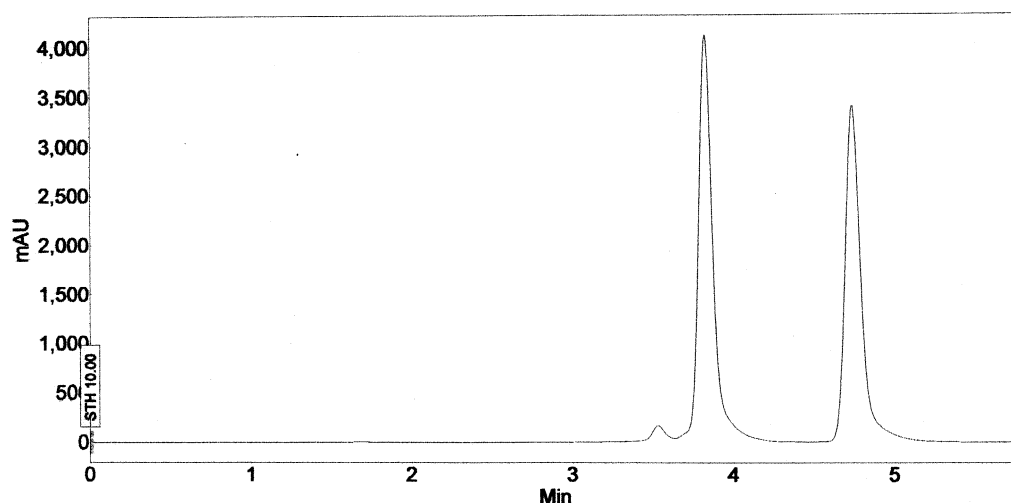
Figure S27. Semipreparative HPLC enantioseparation of **EMAC8000d**; eluent: ethanol-acetonitrile/H_2O 55-40-5 (v/v/v); flow rate: 3.0 mL/min^{-1}; detector UV: 254 and 360 nm; temperature, 25 °C.

After semipreparative separation, the collected fractions were analyzed by chiral column to determine the enantiomeric excess (e.e.). Table shows the enantiomeric excess and rotation specific for pooled fractions containing the first eluted [(+)-**EMAC8000d**)] and second eluted [(-)-(**EMAC8000d**)] enantiomer. Polarimetric analysis indicated that the first eluting enantiomer was dextrorotatory.

Table S4. Chromatographic and polarimetric analysis of the pooled fractions containing the first [(+)-**EMAC8000d**)] and the second [(-)-**EMAC8000d**)] eluted enantiomer of **EMAC8000d**.

Compound	1st eluted enantiomer		2nd eluted enantiomer	
	e.e. (%)	$[\alpha]_D^{25}$	e.e. (%)	$[\alpha]_D^{25}$
EMAC 8000d	>99.0	+58	>99.0	-57

Conditions for the semipreparative enantioseparation: column: Chiralpak IA (250 x 10mm I.D.); eluent: ethanol-acetonitrile/H_2O 55-40-5 (v/v/v); flow rate, 3.0 mL min^{-1}; detector: UV at 254 nm and 360 nm; temperature: 25°C. Amount of sample resolved in a single semipreparative run: about 2 mg. Volume of injection: 0.5 mL.

Molecular Modelling

The ligands were downloaded from the Protein Data Bank (PDB)[1] or built within Maestro GUI.[2] Their geometry was optimized. In particular the compounds were subjected to a conformational search protocol with MacroModel version 7.2,[3] considering MMFFs[4] as force field and considering solvent effects by adopting the implicit solvation model Generalized Born/Surface Area (GB/SA) water.[5] The simulation was performed allowing 5000 steps Monte Carlo analysis with Polak-Ribier Conjugate Gradient (PRCG) method and a convergence criterion of 0.05 kcal/(mol Å).

Protein preparation was performed starting from protein structure model with PDB code 4WW8 using Protein preparation module in Maestro 9.0.[2] All the water molecules were removed. This PDB model was chosen because of his best resolution (1.44 Å) compared to the other available. The protein was subjected to a minimization with Macromodel version 9.2 considering OPLS2005[6] as force field. The simulation was performed allowing 5000 steps Monte Carlo analysis with PRCG method and a convergence criterion of 0.05 kcal/(mol·Å).

Docking experiments were performed by means of Glide Quantum-Mechanical Polarized Docking.[7] The Grid box was centered on the co-crystallized ligand and all parameters were set up as default. Re-docking and cross docking simulations were carried out to validate the protocol. Root-mean square deviation (RMSD) between the crystallographic pose and the best 10 binding poses of each compound ranked by Glide score were calculated (Table S5) (Figure 28).

Validated protocol was then applied to the compound **EMAC8000d, EMAC8000f** and **EMAC8000m** on R and S configuration.

In order to take into account the induced fit phenomena, the best three poses of reference compound, Acetazolamide (**AAZ**), and **EMAC8000d, f, m** enantiomers were subjected to post-docking procedure based on energy minimization and subsequent binding free energies calculation. The free energies of binding were obtained applying molecular mechanics and continuum solvation models using the molecular mechanics Generalized Born/Surface Area (MM-GBSA) method.[7] Depictions were taken with Maestro GUI[2] and Pymol.[8]

Table S5. Cross- and Self- Docking: RMSD values of acetazolamide (AAZ) and 4-propylthiobenzenesulfonamide (VD9) of the 10 poses generated by the docking program.

Compound	RMSD
VD9	**0.89**
VD9	2.02
VD9	2.17
VD9	1.81
VD9	2.36
VD9	2.08
VD9	1.65
VD9	1.58
VD9	1.38
VD9	1.72
AAZ	**1.33**
AAZ	1.38
AAZ	1.32
AAZ	1.32
AAZ	1.32
AAZ	1.32
AAZ	**0.99**
AAZ	1.08
AAZ	1.33
AAZ	1.02
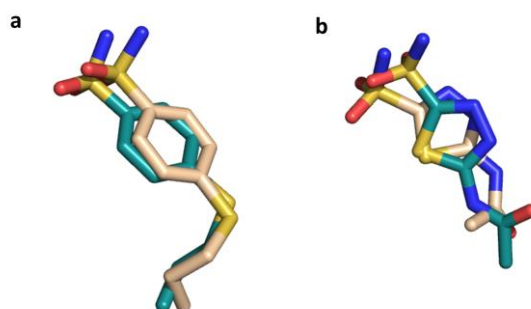
Figure S28. 3D visualization of self and cross-docking results (pdb code 4WW8). In wheat the crystallographic pose and in cyan the docked pose of a) VD9 and b) AAZ.

Table S6: Docking score of the best docking poses of AAZ and VD9

Compound	Docking score (Kcal/mol)
VD9	-9.15
VD9	-9.13
VD9	-8.84
AAZ	-9.61
AAZ	-9.27
AAZ	-9.19

Table S7. Free energies of interaction of complexes resulting from the post-docking procedure and the relative docking scores of reference compound **AAZ**, **EMAC8000d**, **EMAC8000f** and **EMAC8000m**.

Compound	ΔG (Kcal/mol)	Docking score (Kcal/mol)
AAZ (Boltz. 0.07%)	-45.4	-9.61
AAZ (Boltz. 99.93 %)	**-49.38**	-9.27
AAZ (Boltz. 0%)	-39.19	-9.19
(R)-EMAC8000d (Boltz. 1.45 %)	-25.45	-8.45
(R)-EMAC8000d (Boltz. 39.34 %)	-28.35	-8.42
(R)-EMAC8000d (Boltz. 59.21%)	**-28.36**	-8.41
(S)-EMAC8000d (Boltz. 100 %)	**-25.75**	-8.28
(S)-EMAC8000d (Boltz. 0 %)	-21.93	-8.12
(R)-EMAC8000f (Boltz. 37.56 %)	-7.83	-7.29
(R)-EMAC8000f (Boltz. 44.82%)	**-7.75**	-7.28
(S)-EMAC8000f (Boltz. 45.14 %)	**-3.7**	-6.62
(S)-EMAC8000f (Boltz. 31.19 %)	-3.64	-6.54
(R)-EMAC8000m (Boltz. 47.81%)	**-5.45**	-7.22
(R)-EMAC8000m (Boltz. 34.25 %)	-5.45	-7.21
(S)-EMAC8000m (Boltz. 99.69 %)	0.65	-6.38
(S)-EMAC8000m (Boltz. 0.31 %)	**-2.46**	-6.31

```
CA-I    MSPDWGYDDKNGPEQWSKLYPIANGNNQSPVDIKTSETKHDTSLKPISVSY---NPATAK
CA-II   MSHHWGYGKHNGPEHWHKDFPIAKGERQSPVDIDTHTAKYDPSLKPLSVSY---DQATSL
CA-IX   ---HWRY---GGDPPWPRVSPACAGRFQSPVDIRPQLAAFSPALRPLELSGFQLPPLPEL
CA-XII  -MSKWTYFGPDGENSWSKKYPSCGGLLQSPIDLHSDILQYDASLTPLEFQGYNLSANKQF
         .* *   .*   * :  * . *  ***:*:        .. :* *:...

CA-I    EIINVGHSFHVNFEDNDNRSVLKGGPFSDSYRLFQFHFHWGSTNE-HGSEHTVDGVKYSA
CA-II   RILNNGHAFNVEFDDSQDKAVLKGGPLDGTYRLIQFHFHWGSLDG-QGSEHTVDKKKYAA
CA-IX   RLRNNGHSVQLTLPPGLEMK---L-GPGREYRALQLHLHWGAAGRP-GSEHTVEGHRFPA
CA-XII  LLTNNGHSVKLNLPSDMHIQ-----GLQSRYSATQLHLHWGNPNDPHGSEHTVSGQHFAA
         : * **:.:: :  . .          *  *:*:***  .  ******. :: *

CA-I    ELHVAHWNSAKYSSLAEAASKADGLAVIGVLMKVGE-ANPKLQKVLDALQAIKTKGKRAP
CA-II   ELHLVHWNT-KYGDFGKAVQQPDGLAVLGIFLKVGS-AKPGLQKVVDVLDSIKTKGKSAD
CA-IX   EIHVVHLSTK-YARVDEALGRPGGLAVLAAFLEEGPEENSAYEQLLSRLEEIAEEGSETQ
CA-XII  ELHIVHYNSDLYPDASTASNKSEGLAVLAVLIEMGS-FNPSYDKIFSHLQHVKYKGQEAF
        *:*:.* .:  *    *  :  ****:. ::: *   :   :::.. *: :  :*. :

CA-I    FTNFDPSTLLPSSL-DFWTYPGSLTHPPLYESVTWIICKESISVSSEQLAQFRSLLSNVE
CA-II   FTNFDPRGLLPESL-DYWTYPGSLTTPPLLECVTWIVLKEPISVSSEQVLKFRKLNFNGE
CA-IX   VPGLDISALLPSDFSRYFQYEGSLTTPPCAQGVIWTVNFQTVSLSAKQLHTLSDTLWG--
CA-XII  VPGFNIEELLPERTAEYYRYRGSLTTPPCNPTVLWTVFRNPVQISQEQLLALETALYCTH
        . .::   ***.    :: * **** **   * *  : .:  :.:* :*: :

CA-I    --GDNAVPMQHNNRPTQPLKGRTVRASF---------
CA-II   --GEPEELMVDNWRPAQPLKNRQIKASFK--------
CA-IX   ---PGDSRLQLNFRATQPLNGRVIEASFPAGVDSSPR
CA-XII  MDDPSPREMINNFRQVQKFDERLVYTSFSQ-------
        : * * .* :. * : :**
```
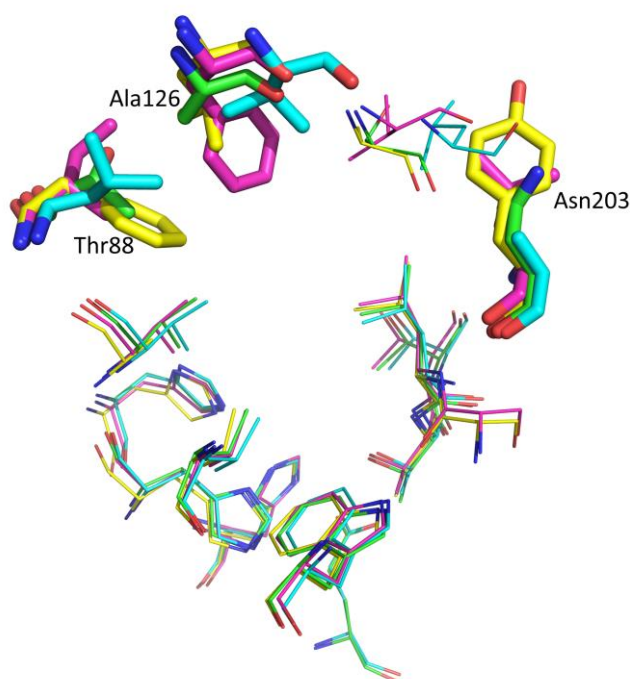
Figure S29. Multiple sequence alignment between the sequence of hCA I, II, IX, XII obtained with ClustalO.[9] The relevant differences between the four isoforms in the binding site are highlighted in red.

Figure S30. Comparison between the binding sites of hCA I (yellow), hCA II (magenta), hCA IX (cyan) and hCA XII (green). In sticks the most relevant differences between the four isoforms, residue number is referred to hCAXII.
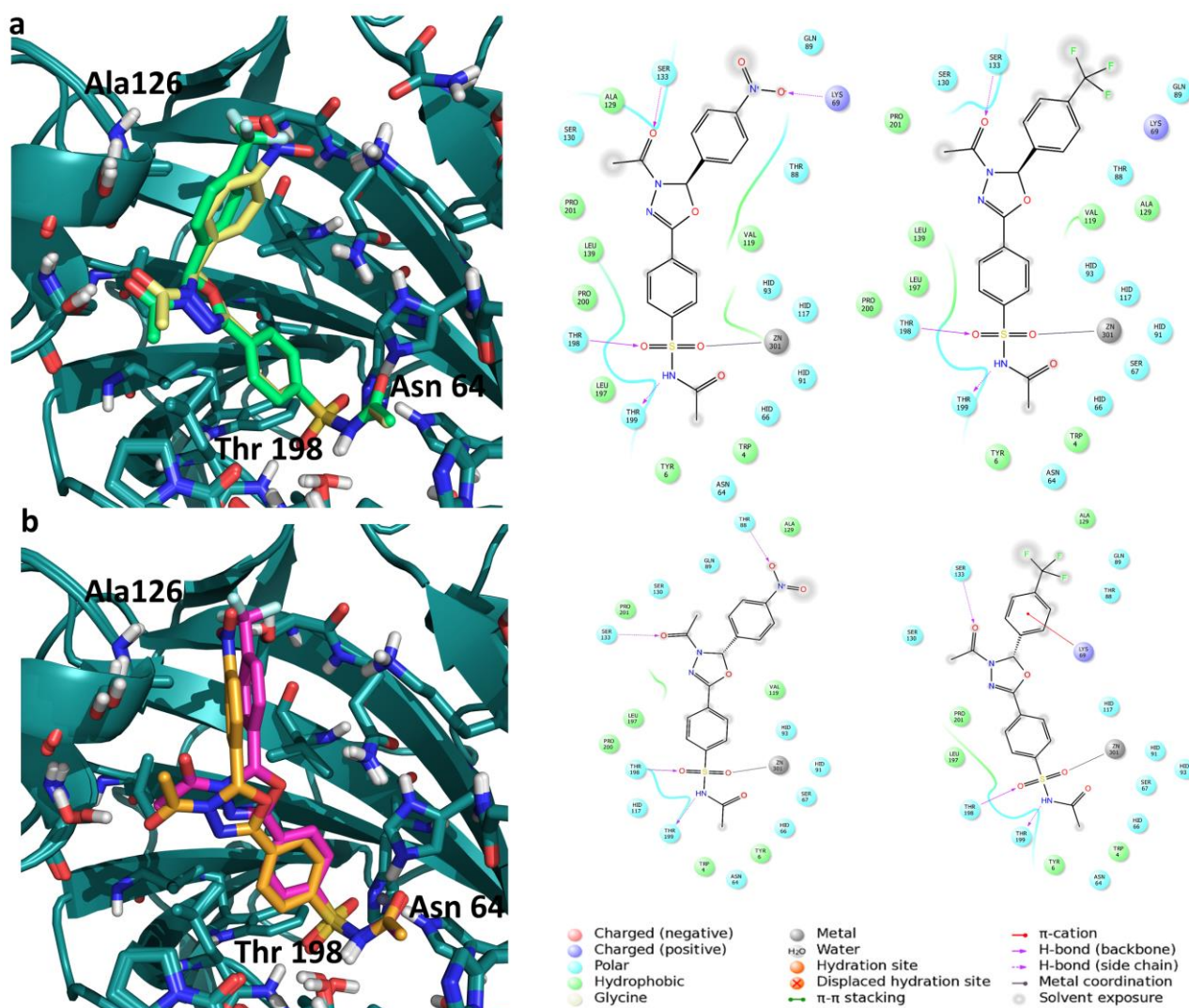
Figure S31. a) 3D representation of the putative binding mode obtained by docking experiment of **(R)-EMAC8000f** (yellow) and **(R)-EMAC8000m** (green) into hCA XII (pdb code 4WW8) with the respective 2D representations. b) 3D representation of the putative binding mode of **(S)-EMAC8000f** (orange) and **(S)-EMAC8000m** (magenta) with the respective 2D representations.

CA inhibition studies

An applied photophysics stopped-flow instrument has been used for assaying the CA catalyzed CO_2 hydration activity.[10] Phenol red (at a concentration of 0.2 mM) has been used as indicator, working at the absorbance maximum of 557 nm, with 20 mM Hepes (pH 7.4) and 20 mM NaBF4 (for maintaining constant the ionic strength), following the initial rates of the CA-catalyzed CO_2 hydration reaction for a period of 10-100 s. The CO_2 concentrations ranged from 1.7 to 17 mM for the determination of the kinetic parameters and inhibition constants. For each inhibitor, at least six traces of the initial 5-10% of the reaction have been used for determining the initial velocity. The un-catalyzed rates were determined in the same manner and subtracted from the total observed rates. Stock solutions of inhibitor (10 mM) were prepared in distilled-deionized water and dilutions up to 0.01 nM were done thereafter with distilled-deionized water. Inhibitor and enzyme solutions were pre-incubated together for 15 min at RT prior to assay, in order to allow for the formation of the E-I complex. The inhibition constants were obtained by non-linear least squares methods using PRISM 3, whereas the kinetic parameters for the uninhibited enzymes from Lineweaver-Burk plots, as reported earlier,[10-12] and represent the mean from at least three different determinations. All CAs were recombinant proteins obtained as reported earlier by these groups.[13]

References

(1)   Berman, H. M.; Westbrook, J.; Feng, Z.; Gilliland, G.; Bhat, T. N.; Weissig, H.; Shindyalov, I. N.; Bourne, P. E. The protein data bank. *Nucleic Acids Res.* **2000,** *28*, 235-242.

(2)   Schrödinger LLC.: New York, N., USA, .

(3)   Mohamadi, F.; Richards, N. G.; Guida, W. C.; Liskamp, R.; Lipton, M.; Caufield, C.; Chang, G.; Hendrickson, T.; Still, W. C. MacroModel—an integrated software system for modeling organic and bioorganic molecules using molecular mechanics. *J. Comput. Chem.* **1990,** *11*, 440-467.

(4)   Halgren, T. A. Merck molecular force field. II. MMFF94 van der Waals and electrostatic parameters for intermolecular interactions. *J. Comput. Chem.* **1996,** *17*, 520-552.

(5)   Still, W. C.; Tempczyk, A.; Hawley, R. C.; Hendrickson, T. Semianalytical treatment of solvation for molecular mechanics and dynamics. *J. Am. Chem. Soc.* **1990,** *112*, 6127-6129.

(6)   Jorgensen, W. L. OPLS force fields. *Encyclopedia of computational chemistry* **1998**.

(7)   Chung, J. Y.; Hah, J. M.; Cho, A. E. Correlation between performance of QM/MM docking and simple classification of binding sites. *J. Chem. Inf. Model.* **2009,** *49*, 2382-7.

(8)   The PyMOL Molecular Graphics System, V. S., LLC.

(9)   Sievers, F.; Wilm, A.; Dineen, D.; Gibson, T. J.; Karplus, K.; Li, W.; Lopez, R.; McWilliam, H.; Remmert, M.; Söding, J.; Thompson, J. D.; Higgins, D. G. Fast, scalable generation of high-quality protein multiple sequence alignments using Clustal Omega. *Mol. Syst. Biol.* **2011,** *7*.

(10)   Khalifah, R. G. Carbon dioxide hydration activity of carbonic anhydrase. I. Stop-flow kinetic studies on the native human isoenzymes B and C. *J. Biol. Chem.* **1971,** *246*, 2561-73.

(11)   Neri, D.; Supuran, C. T. Interfering with pH regulation in tumours as a therapeutic strategy. *Nat. Rev. Drug Discovery* **2011,** *10*, 767-777.

(12)   Supuran, C. T. Carbonic anhydrase inhibitors and activators for novel therapeutic applications. *Future Med. Chem.* **2011,** *3*, 1165-1180.

(13)   Supuran, C. T.; Mincione, F.; Scozzafava, A.; Briganti, F.; Mincione, G.; Ilies, M. A. Carbonic anhydrase inhibitors. Part 52. Metal complexes of heterocyclic sulfonamides: a new class of strong topical intraocular pressure-lowering agents in rabbits. *Eur. J. Med. Chem.* **1998,** *33*, 247-254.